PHYSICAL REVIEW C VOLUME 13, NUMBER 4 APRIL 1976

Ground state properties of medium-heavy nuclei with a realistic interaction

A. L. Goodman*
Carnegie-Mellon University, Pittsburgh, Pennsylvania 15213

J. P. Vary†
Ames Laboratory, Energy Research and Development Administration and Department of Physics, Iowa State University, Ames, Iowa 50010‡
and Brookhaven National Laboratory, Upton, New York 11973

R. A. Sorensen*
Carnegie-Mellon University, Pittsburgh, Pennsylvania 15213
(Received 29 September 1975)

The Brueckner G matrix appropriate for medium-heavy nuclei is obtained from the Reid soft-core nucleon-nucleon potential. The G matrix is strongly affected by the Pauli operator Q, which is treated exactly (no angle averaging). Within the range of valence space energies G has a weak dependence on the starting energy ω. Ground state properties of deformed rare earth nuclei ($Z = 64$–76, $N = 90$–102) and spherical semimagic nuclei (Sn, Pb, $N = 82$, $N = 126$) have been calculated in the Hartree-Fock-Bogoliubov approximation with an inert core of 110 nucleons. Deformations and pair gaps are both determined by the G matrix. The systematic experimental dependence of $\epsilon_{\text{spherical}}$, β_2, β_4, Δ_p, Δ_n, and E_{po} (prolate-oblate energy difference) on N and Z is reproduced. However, the magnitudes of β_2, Δ_n, and E_{po} are too small. This may be largely due to the lack of isospin dependence of the oscillator basis states. β_2 and E_{po} could receive additional significant contributions from core polarization of the 110 particle core which is neglected here. The Hartree-Fock-Bogoliubov ground states obtained with this realistic interaction provide a reasonable foundation for high spin calculations.

[NUCLEAR STRUCTURE Brueckner reaction matrix; Hartree-Fock-Bogoliubov theory; ground state properties of medium-heavy nuclei.]

I. INTRODUCTION

One of the most fundamental and challenging problems in nuclear physics has been to develop a microscopic theory of the structure of finite nuclei in terms of the nucleon-nucleon interaction and basic many body theory.

The interesting problems of nuclear structure require an understanding of the different collective modes and their mutual interaction. With the use of the formalism to be described, we expect to derive properties of certain classes of nuclear excited states as well as of ground states from the two-body interaction.

A current problem of particular interest is the rapid increase in moment of inertia of rare-earth nuclei at about spin $14\hbar$. This phenomenon involves the single-particle and pairing properties as well as the deformed field aspects of nuclear structure. It is the ultimate aim of this research to perform a theoretical calculation of such effects using a force derived from two nucleon data.

This paper reports calculations of the ground state properties including single-particle energies, pairing and quasiparticle energies, and deformation energies and shapes for the region from $82 \leq N \leq 126$ and $50 \leq Z \leq 82$, based on the Reid soft-core potential.[1] The high spin states will be treated in a subsequent publication.

Earlier calculations by Kumar and Baranger[2] used the schematic pairing plus quadrupole force. More recent calculations for this region use Skyrme type forces,[3] which are related to the two-body force, but contain parameters chosen so that the binding energy and density of nuclear matter and selected spherical nuclei are reproduced. The Skyrme interaction is used to calculate only the Hartree-Fock (HF) field and deformations. The pairing gap is inserted with the usual phenomenological pairing force. In neither of the above methods is the effective interaction explicitly derived from the nucleon-nucleon potential, nor are the deformations and pair gaps both determined by the same interaction.

It is not currently feasible to perform a fully self-consistent Brueckner-Hartree-Fock calculation with pairing correlations included for heavy nuclei with a realistic force. Likewise, a shell model calculation (using a realistic effective force) in a space adequate to describe the properties of interest for these nuclei is not presently possible.

In this calculation, the Brueckner ladder summation is used to generate from the Reid soft-

core potential an effective interaction. A large valence space is selected and the interaction is suitable as a shell model force in the rare-earth region, as described in Sec. II. We are aware of the problems with the convergence of the effective interaction expansion, but hope that our subsequent dynamical calculation of the collective pairing and deformation effects may ease some of those problems.

In Sec. III a Hartree-Fock-Bogoliubov (HFB) calculation is made, in which the deformation and pairing effects are simultaneously treated self-consistently with the same effective interaction. The HFB equations are solved in the large valence space (with the remaining core furnishing fixed single particle energies). We hope, of course, that the HFB will approximate an exact shell model diagonalization. Since the valence space contains only one single-particle state for each combination of orbital, spin, and isospin quantum numbers, only angular and not radial self-consistency is achieved. The resulting ground state properties are then compared with actual deformed rare-earth nuclei in Sec. IV. In Sec. V the same formalism is applied to the spherical semimagic nuclei surrounding the rare-earth nuclei in the Isotope Chart, and compared with experiment. Section VI lists the conclusions.

II. REALISTIC EFFECTIVE INTERACTION

We wish to emphasize again that this application of a realistic effective interaction bridges a gap between two conventional domains. Namely, we bridge the Brueckner-Hartree-Fock and shell model domains by treating with a realistic interaction a large number of quasiparticles self-consistently within a large valence space. We do so fully aware of the problems with realistic effective interactions in both domains but with the strong conviction that those problems even motivate the present effort.

A. Theory and method of solution

The Brueckner effective interaction $G(\omega)$ is derived from the realistic nucleon-nucleon interaction V and represents an infinite (ladder) series summation of the strong V interactions. By summing the more pathological diagrams directly, it is hoped that the renormalized force obtained will be suitable for structure calculations. The series is evaluated through solving the Brueckner-Bethe-Goldstone equation:

$$G(\omega) = V + V\frac{Q}{\omega - H_0} G(\omega) , \tag{2.1}$$

where Q is the two-particle Pauli operator which forbids those intermediate two-particle states that are either normally occupied (either nucleon in a "core" state) or that will be treated directly in the dynamical framework (both nucleons in "valence" states). ω is the "starting energy" which is determined self-consistently in a Brueckner-Hartree-Fock (BHF) application. In the shell-model (SM) situation it is either determined self-consistently (Brillouin-Wigner type perturbation theory) or taken as a constant or average value (Rayleigh-Schrödinger type). H_0 is the single-particle Hamiltonian which is usually chosen self-consistently (BHF) or on physical intuition, as in some SM applications, or for convenience, as in other SM cases.

It is convenient to solve this equation by first solving for a reference interaction $G^R(\omega)$,

$$G^R(\omega) = V + V\frac{1}{\omega - H_0} G^R(\omega) , \tag{2.2}$$

to accommodate the main effects of short-range correlations in a representation with all the symmetries of V. Then one incorporates the long-range symmetry-breaking Pauli operator via the identity

$$G(\omega) = G^R(\omega) + G^R(\omega)\left(\frac{Q}{\omega - H_0} - \frac{1}{\omega - H_0}\right)G(\omega) . \tag{2.3}$$

The propagator $1/(\omega - H_0)$ is chosen for convenience and, in principle, another operator could stand in its place in the last two equations.

Convenient methods[4,5] for solving (2.2) are known when H_0 is a harmonic oscillator. Some[4] are especially useful when V is the Reid soft-core interaction,[1] while another[5] is more suited for the hard-core Hamada-Johnston interaction.[6] These methods can be understood by rewriting (2.2) as the identity

$$G^R(\omega) = (H_0 - \omega) + (H_0 - \omega)\frac{1}{\omega - H_0 - V}(H_0 - \omega) . \tag{2.4}$$

By expanding the denominator one obtains the same series as (2.2).

The infinite dimension problem (2.4) must be truncated in order to be numerically tractable and is evaluated in the relative center of mass representation. For a soft-core interaction, where the matrix elements of V may be directly evaluated in the harmonic oscillator representation, one method[4] is to truncate the infinite matrix $(\omega - H_0 - V)$, invert it, and perform the remaining matrix operations in (2.4). Another equivalent

method[4] is to diagonalize the truncated matrix (H_0+V) to obtain the eigenvalues E_i and eigenvectors $|\psi_i\rangle$,

$$(H_0+V)|\psi_i\rangle = E_i|\psi_i\rangle \tag{2.5}$$

in an oscillator expansion

$$|\psi_i\rangle = \sum_\alpha \langle\alpha|\psi_i\rangle|\alpha\rangle\,, \tag{2.6}$$

so that matrix elements of (2.4) are given by

$$\langle\alpha|G^R(\omega)|\beta\rangle = (\epsilon_\alpha-\omega)\left[\delta_{\alpha,\beta}+\sum_i \frac{\langle\alpha|\psi_i\rangle\langle\psi_i|\beta\rangle}{\omega-E_i}(\epsilon_\beta-\omega)\right]. \tag{2.7}$$

With the same truncation the above two methods must yield the same results.

In the case of a hard-core interaction the method proposed[5] was to numerically solve the Schrödinger equation (2.5) and evaluate the overlap integrals in (2.6), then proceed with (2.7).

The method employed here is matrix diagonalization, since that is performed once, and $G^R(\omega)$ may be evaluated for many values of ω by simple matrix manipulations.

Various approximations have been introduced in the past to treat the Pauli operator in a simple fashion. Becker, MacKellar, and Morris[36,37] were the first to draw attention to a possible need for an exact treatment of Q. However, since that time little has been done to check these approximations with exact results except in an investigation of mass 18 two-particle spectra[5] and in mass 16 binding energy calculations.[7] Some differences are observed. However, in medium-heavy nuclei Q blocks far more phase space and plays a much more dramatic role in determining G. That is, the differences between G and G^R are far greater in medium-heavy nuclei than they are in light nuclei because of the larger deviation of Q from the identity operator (compare Tables II and III below). Since Q enters in a nonlinear fashion in (2.3) and since this nonlinearity increases with the importance of Q, it is difficult and dangerous to extrapolate the mass 16 and 18 tests to an estimate of the acceptability of a given approximation of Q in medium and heavy mass situations. In addition, Barrett, Hewitt, and McCarthy[5,7] have emphasized that those applications which deal directly with surface effects are the ones where approximations to Q will be least reliable.

Early estimates indicated an exact treatment of Q with sufficient accuracy in the single-particle basis might be technically feasible. However, the method of Ref. 5 (also used in Ref. 4) for evaluating (2.3) would be inadequate here due to the large asymmetric matrices involved. Thus, alternative methods were outlined and attempted. The most reliable and the most economical in terms of computer storage usage was to rewrite (2.3) with

$$S \equiv \left(\frac{Q}{\omega-H_0}-\frac{1}{\omega-H_0}\right), \tag{2.8}$$

then

$$G = G^R + G^R S G$$

rearranging

$$(1-G^R S)G = G^R$$

and multiplying both sides by $(G^R)^{-1}$

$$[(G^R)^{-1}-S]G = 1\,,$$

so that, solving for G,

$$G = [(G^R)^{-1}-S]^{-1}. \tag{2.9}$$

Storage economy is achieved, since this is a succession of symmetric (but indefinite) matrix inversion operations.

B. Parameter selection, approximations, and validity tests

We next introduce the ingredients selected for the calculations. At the same time, when convenient, we comment on these selections and mention the more salient limitations. Approximations are also introduced and discussed briefly. Then, at the end of the chapter, we check the validity of those approximations for which it was feasible to run a test calculation.

The Reid soft-core potential was selected and its major limitation for our purposes would appear to be that it only includes those partial waves of total relative angular momentum $\mathcal{J}$ through $\mathcal{J}=2$. Future efforts should include at least a one-pion exchange potential in the higher partial waves.

For H_0 we selected a pure harmonic oscillator with $\hbar\Omega = 7.5$ MeV. It would certainly be desirable to have a different oscillator well for the neutrons and the protons in order to more closely approximate the physical situation. However, this additional complexity, if treated exactly would render the present application unfeasible at this time. Approximations are under investigation to remedy this deficiency.

The valence space for these calculations contains seven orbitals for the protons ($3s_{1/2}, 2d_{5/2}, 2d_{3/2}, 1g_{9/2}, 1g_{7/2}, 1h_{11/2}, 1h_{9/2}$) and can accommodate 52 protons. For the neutrons we include eight orbitals ($3p_{3/2}, 3p_{1/2}, 2f_{7/2}, 2f_{5/2}, 1h_{11/2}, 1h_{9/2}, 2g_{9/2}, 1i_{13/2}$) which can hold 66 neutrons.

The inert core therefore consists of 40 protons and 70 neutrons.

Isospin dependence of the oscillator is expected to be the major effect of all the isospin dependence on the effective interaction. By choosing oscillator constants such that the unperturbed rms radii of the distributions of neutrons and protons will be the same in a given nucleus, we will *increase* the ratio of neutron-neutron to proton-proton effective interaction strength. A crude estimate of the size of this effect will be shown below in Sec. IV E to significantly *increase* the over-all magnitudes of collective strengths in these nuclei towards better agreement with experiment.

Another approximation we have made is to take an isospin independent Pauli operator. However, the selection is made in such a way as to partially cancel the error made by choosing an isospin independent oscillator. That is, the isospin independent boundaries between core and valence states and between valence and unoccupied states are drawn to underestimate the neutron core space and to overestimate the proton valence space. Removing this approximation alone will *decrease* the ratio of neutron-neutron to proton-proton effective interaction strength.

Note that the Pauli operator is defined in the shell model manner rather than in the Brueckner-Hartree-Fock manner. Full self-consistency would require an additional Pauli excluded space of two-particle states consisting of an occupied valence orbital and an orbital in the region beyond the valence space. However, the basis space within which the Pauli operator is defined is self-consistent with it, since radial wave functions are not varied.

The shell model choice represents a convenience. It may also be argued that since we are only attempting HFB in a large valence space, we are seeking an approximation to a large shell model diagonalization and this motivates the choice of the effective operator.

The starting energy ω was chosen to correspond to an average binding energy of 10 MeV for the bound valence single-particle states. Thus, for practical reasons, we sacrificed the self-consistent ω selection process which is known to be important in Brueckner-Hartree-Fock calculations of total binding energy and total density. This appears to be reasonable in the present application which aims primarily at relative surface properties for two reasons: First, only the valence nucleons are treated self-consistently in the HFB calculations, and their binding energies are found to be spread about 10 MeV around our average choice; second, the ω dependence of G within this limited range is found to be fairly weak (see Table I).

The matrix diagonalization problem in (2.4) was truncated at the dimension 110×110 for all partial waves. Such a truncation was found to be very accurate[4] for the slowest converging eigenvalue when compared to the eigenvalue obtained from directly solving the Schrödinger equation. Increasing this space by a factor of 2, if it were feasible, might be expected to affect the G matrix elements we use by as much as 2%. This certainly represents one of the more minor approximations.

The matrix inversion problem (2.9) must also be truncated. Experience has shown[4,5] that it is sufficient to include unoccupied states through two major shells beyond the valence space. That this should be true more or less independent of the region of the Periodic Table in which one is working can be seen from the following argument. On the one hand, as one goes to heavier nuclei the oscillator spacing is decreasing making it energetically easier to couple to the unoccupied space which would indicate a need to *increase* the unoccupied space. On the other hand, the phase space in each unoccupied shell is increasing and the average matrix element coupling to that space is decreasing both of which *reduce* the need for a larger unoccupied space. The net effect is to preserve the two shell estimate as a valid truncation (see Table I).

We now illustrate with test calculations the possible importance of some of these approximations. We select the $J^\pi=0^+$, $T=1$ matrix and study those matrix elements involving neutron valence orbitals. The results of four separate calculations are displayed in Table I. Column A gives the matrix elements from the full calculation as described above. These are the actual results employed in the HFB calculations.

In column B we portray the effect of increasing the isospin independent core orbital space to include *all* the orbitals up to the lower limit of the neutron valence space. This nearly doubles the occupied space from 80 nucleons to 140 nucleons. Typically, this reduces the absolute strengths from a few percent to 10% with important exceptions. Those matrix elements involving the $|2g_{9/2}, 1g_{9/2}\rangle$ basis state are more dramatically affected. In column A these are both valence orbitals but with this change of Pauli operator the $1g_{9/2}$ has been shifted to the core space. Intuitively, such a change of status may be expected to have the more dramatic consequences that are indeed observed. Otherwise, the changes in the remaining matrix elements in going from column A to column B verify the fact that the isospin dependence of Q is a less important effect than the isospin dependence of the oscillator constants (shown in Sec

TABLE I. Elements of the $J^\pi = 0^+, T=1$ submatrix involving single-particle orbitals in the neutron valence space. Column A gives the matrix elements employed in the HFB studies. Column B displays the effect of enlarging the core space to include the lowest 140 nucleon orbitals. Column C shows the additional effect of making ω 15 MeV smaller (7.5 MeV more binding per valence orbital). In Column D one has, in addition to the effects of columns B and C, the effect of adding two more major shells to the unoccupied space beyond the valence space for the truncated inversion of (2.9).

$\langle x \mid y \rangle$					
x	y	A	B	C	D
$2g_{9/2}1g_{9/2}$	$2g_{9/2}1g_{9/2}$	−0.798	−0.656	−0.582	−0.576
$2g_{9/2}1g_{9/2}$	$(3p_{3/2})^2$	−0.192	−0.172	−0.165	−0.167
$2g_{9/2}1g_{9/2}$	$(3p_{1/2})^2$	−0.106	−0.087	−0.082	−0.084
$2g_{9/2}1g_{9/2}$	$(2f_{7/2})^2$	−0.447	−0.424	−0.415	−0.413
$2g_{9/2}1g_{9/2}$	$(2f_{5/2})^2$	−0.203	−0.160	−0.144	−0.142
$2g_{9/2}1g_{9/2}$	$(1h_{11/2})^2$	−0.322	−0.301	−0.297	−0.296
$2g_{9/2}1g_{9/2}$	$(1h_{9/2})^2$	−0.128	−0.099	−0.089	−0.088
$2g_{9/2}1g_{9/2}$	$(2g_{9/2})^2$	0.295	0.295	0.298	0.299
$2g_{9/2}1g_{9/2}$	$(1i_{13/2})^2$	0.480	0.426	0.403	0.401
$(3p_{3/2})^2$	$(3p_{3/2})^2$	−0.589	−0.567	−0.525	−0.514
$(3p_{3/2})^2$	$(3p_{1/2})^2$	−0.649	−0.635	−0.614	−0.609
$(3p_{3/2})^2$	$(2f_{7/2})^2$	−0.308	−0.291	−0.270	−0.270
$(3p_{3/2})^2$	$(2f_{5/2})^2$	−0.320	−0.307	−0.293	−0.292
$(3p_{3/2})^2$	$(1h_{11/2})^2$	−0.202	−0.200	−0.185	−0.187
$(3p_{3/2})^2$	$(1h_{9/2})^2$	−0.224	−0.221	−0.212	−0.214
$(3p_{3/2})^2$	$(2g_{9/2})^2$	0.395	0.372	0.343	0.339
$(3p_{3/2})^2$	$(1i_{13/2})^2$	0.245	0.235	0.215	0.217
$(3p_{1/2})^2$	$(3p_{1/2})^2$	−0.128	−0.115	−0.089	−0.082
$(3p_{1/2})^2$	$(2f_{7/2})^2$	−0.278	−0.269	−0.257	−0.256
$(3p_{1/2})^2$	$(2f_{5/2})^2$	−0.154	−0.141	−0.129	−0.129
$(3p_{1/2})^2$	$(1h_{11/2})^2$	−0.193	−0.190	−0.183	−0.184
$(3p_{1/2})^2$	$(1h_{9/2})^2$	−0.101	−0.099	−0.091	−0.092
$(3p_{1/2})^2$	$(2g_{9/2})^2$	0.347	0.331	0.314	0.310
$(3p_{1/2})^2$	$(1i_{13/2})^2$	0.226	0.216	0.205	0.206
$(2f_{7/2})^2$	$(2f_{7/2})^2$	−0.555	−0.535	−0.485	−0.479
$(2f_{7/2})^2$	$(2f_{5/2})^2$	−0.959	−0.945	−0.921	−0.918
$(2f_{7/2})^2$	$(1h_{11/2})^2$	−0.296	−0.293	−0.264	−0.266
$(2f_{7/2})^2$	$(1h_{9/2})^2$	−0.498	−0.491	−0.479	−0.480
$(2f_{7/2})^2$	$(2g_{9/2})^2$	0.388	0.367	0.322	0.318
$(2f_{7/2})^2$	$(1i_{13/2})^2$	0.360	0.349	0.314	0.314
$(2f_{5/2})^2$	$(2f_{5/2})^2$	−0.264	−0.242	−0.205	−0.200
$(2f_{5/2})^2$	$(1h_{11/2})^2$	−0.493	−0.486	−0.473	−0.474
$(2f_{5/2})^2$	$(1h_{9/2})^2$	−0.157	−0.151	−0.133	−0.135
$(2f_{5/2})^2$	$(2g_{9/2})^2$	0.744	0.731	0.710	0.708
$(2f_{5/2})^2$	$(1i_{13/2})^2$	0.563	0.545	0.526	0.526
$(1h_{11/2})^2$	$(1h_{11/2})^2$	−0.596	−0.582	−0.516	−0.514
$(1h_{11/2})^2$	$(1h_{9/2})^2$	−1.469	−1.458	−1.435	−1.435
$(1h_{11/2})^2$	$(2g_{9/2})^2$	0.147	0.151	0.122	0.125
$(1h_{11/2})^2$	$(1i_{13/2})^2$	0.462	0.447	0.383	0.382
$(1h_{9/2})^2$	$(1h_{9/2})^2$	−0.279	−0.265	−0.218	−0.216
$(1h_{9/2})^2$	$(2g_{9/2})^2$	0.430	0.432	0.423	0.425
$(1h_{9/2})^2$	$(1i_{13/2})^2$	1.318	1.303	1.282	1.282
$(2g_{9/2})^2$	$(2g_{9/2})^2$	−0.426	−0.388	−0.332	−0.325
$(2g_{9/2})^2$	$(1i_{13/2})^2$	−0.213	−0.209	−0.175	−0.177
$(1i_{13/2})^2$	$(1i_{13/2})^2$	−0.403	−0.377	−0.308	−0.306

IV E).

Now keeping this new Pauli operator, we show in column C the additional effect in increasing the starting energy by 75% from 10 MeV/nucleon average binding to 17.5 MeV/nucleon. Whereas the choice of a single fixed value of ω is purely for convenience, it is encouraging that the shift in the G matrix elements for a representative change in ω are fairly minor. By representative we mean a change consistent with the range of energy variation in the self-consistent orbitals of this calculation. This also suggests a path for correcting this deficiency of the present calculations via perturbation theory to first order. That is, we could employ

$$G(\omega') \simeq G(\omega) + (\omega' - \omega)\frac{\partial G}{\partial \omega}\bigg|_{\omega},$$

where the second term appears to be, *at most*, about 10% of the first term. The systematic effect this correction would have on average is to *increase* the absolute strength of matrix elements involving two-particle states with starting energy ω' above the average choice ω [$(\omega' - \omega)$ is positive], while decreasing the absolute strength of matrix elements involving two-particle states with ω' below ω [$(\omega' - \omega)$ is negative]. It would certainly be desirable to incorporate such a systematic effect when feasible in future calculations.

It is interesting to contrast the weak starting energy dependence observed here with the strong dependence observed[4,5] in light nuclei. The strongest energy dependence originates in the $^3S_1 - {}^3D_1$ and $^1S_0$ partial waves. Here, the deuteron pole and the low energy scattering "resonance," respectively, dominate the on-shell and near off-shell strong energy dependence of the effective interactions. The amount of this strong energy dependence that survives in the realistic effective interaction as a function of the size of the nuclear medium is dependent on two factors. The leading effect appears to be the fact that a typical two-particle valence space matrix element has decreasing parentage on the lowest partial waves with increasing valence shell quanta. Thus, for example, the matrix element $\langle 1s_{1/2}{}^2 J=0, T=1 | G(\omega) | 1s_{1/2}{}^2 J=0, T=1\rangle$ in a scheme where G possesses a partial wave decomposition is *entirely* the $^1S_0$ component of G which itself (for an angle averaged Q operator) is entirely dependent on the strongly energy dependent $^1S_0$ component of $G^R(\omega)$. However, in the *sd* shell, one might inspect the $\langle 2s_{1/2}{}^2 J=0, T=1 | G(\omega) | 2s_{1/2}{}^2 J=0, T=1\rangle$ matrix element for comparison and there, we find that already the parentage on the $^1S_0$ component of $G^R(\omega)$ has dropped to 21%. Naturally, as one proceeds to the rare-earth valence space the parentage of typical matrix elements on these more troublesome components of the effective interaction will be even further reduced.

A secondary effect on the ω dependence that depends on the system under consideration is the location of the poles in $G(\omega)$. Specifically, we consider the leading $T=0$ pole in the $^3S_1$-$^3D_1$ partial wave in $G^R(\omega)$ itself. For this purpose it is convenient to rewrite (2.2) as

$$G^R(\omega) = V + V\frac{1}{\omega - H_0 - V}V = V + V\frac{1}{\omega - T - U - V}V \tag{2.10}$$

in order to cleanly isolate the analytic ω dependence. The location of the pole depends on the choice of U which is an oscillator in our case. How does the pole location depend on the oscillator constant? To see this we insert a complete set of two-particle states whose relative wave functions are exact solutions of the two-body problem

$$(T_{\rm rel} + V)|\xi_i\rangle = E_i|\xi_i\rangle,$$

where E_0 and $|\xi_0\rangle$ represent the deuteron binding energy and wave function, respectively. The center of mass wave functions will be chosen as appropriate eigenstates of the simple oscillator. Then, if we use

$$T + U + V = (T_{\rm rel} + V) + U_{\rm rel} + (T_{\rm c.m.} + U_{\rm c.m.}), \tag{2.11}$$

the leading $^3S_1$-$^3D_1$ pole ω_0 will be approximately at

$$\omega_0 \cong E_0 + \langle \xi_0 | U_{\rm rel} | \xi_0\rangle + E_{\rm c.m.}, \tag{2.12}$$

where $E_{\rm c.m.}$ represents the oscillator center of mass energy. In the full problem, i.e., in $G(\omega)$, the Pauli operator blocks the low lying c.m. states for this partial wave so the smallest $E_{\rm c.m.}$ that enters is the total oscillator quanta for two particles just *above* the valence space. However, $E_{\rm c.m.}$ is largely canceled by the choice of ω which achieves a net starting energy for each valence particle of -10 MeV to coincide with the selection we indicated above. Thus, the role of $E_{\rm c.m.}$ will always be rather minimal. The other system dependent repulsive shift is $\langle \xi_0 | U_{\rm rel} | \xi_0\rangle$ which may be evaluated

$$\langle \xi_0 | U_{\rm rel} | \xi_0\rangle = \tfrac{1}{2}\mu\Omega^2\langle \xi_0 | r^2 | \xi_0\rangle \tag{2.13}$$

$$\cong 54/A^{2/3}\ \text{MeV}, \tag{2.14}$$

where μ is the reduced nucleon mass, and we have used 2.2 fm as the rms radius of the deuteron and $43/A^{1/3}$ as the mass dependence of the oscillator constant. Thus for $A=16$ this is about 8 MeV and for $A=160$ it is about 2 MeV. On the whole then, ω_0 goes from about $+6$ MeV $+ E_{\rm c.m.}$ to

TABLE II. Comparison of $G^R(\omega)$ in column A with $G(\omega)$ in column B for a part of the submatrix shown in Table I, the first row and then only the diagonal elements.

$\langle x \mid y \rangle$			
x	y	A	B
$2g_{9/2}1g_{9/2}$	$2g_{9/2}1g_{9/2}$	−11.437	−0.798
$2g_{9/2}1g_{9/2}$	$(3p_{3/2})^2$	0.440	−0.192
$2g_{9/2}1g_{9/2}$	$(3p_{1/2})^2$	0.335	−0.106
$2g_{9/2}1g_{9/2}$	$(2f_{7/2})^2$	−9.339	−0.447
$2g_{9/2}1g_{9/2}$	$(2f_{5/2})^2$	−7.941	−0.203
$2g_{9/2}1g_{9/2}$	$(1h_{11/2})^2$	−6.290	−0.322
$2g_{9/2}1g_{9/2}$	$(1h_{9/2})^2$	−5.619	−0.128
$2g_{9/2}1g_{9/2}$	$(2g_{9/2})^2$	4.239	0.295
$2g_{9/2}1g_{9/2}$	$(1i_{13/2})^2$	8.173	0.480
$(3p_{3/2})^2$	$(3p_{3/2})^2$	−0.809	−0.589
$(3p_{1/2})^2$	$(3p_{1/2})^2$	−0.265	−0.128
$(2f_{7/2})^2$	$(2f_{7/2})^2$	−8.224	−0.555
$(2f_{5/2})^2$	$(2f_{5/2})^2$	−6.048	−0.264
$(1h_{11/2})^2$	$(1h_{11/2})^2$	−4.523	−0.596
$(1h_{9/2})^2$	$(1h_{9/2})^2$	−3.625	−0.279
$(2g_{9/2})^2$	$(2g_{9/2})^2$	−2.077	−0.426
$(1i_{13/2})^2$	$(1i_{13/2})^2$	−6.315	−0.403

about $0+E_{\text{c.m.}}$ in going from mass 16 to mass 160. Correspondingly, the smallest energy denominator, when ω is chosen according to our method, goes from $\omega-\omega_0=(-10-10)-6$ to $(-10-10)-0$ which is less than a 25% change. This is the reason for categorizing the location of the poles of $G(\omega)$ as a secondary effect by comparison with the parentage consideration. The above two effects together seem to be consistent with the rather weakened energy dependence of $G(\omega)$ that we find here.

We now consider one final test calculation. While maintaining the two modifications introduced in columns B and C of Table I we show the additional effect in column D of expanding the unoccupied single particle space of the matrix inversion problem (2.9) to include two more major shells. This more than doubles the number of two-particle states involving one nucleon in a core (occupied) orbital and one in the unoccupied space beyond the valence states. Most matrix elements change by only a few keV with the largest change being 11 keV for the diagonal $|3p_{3/2}\ 3p_{3/2}\rangle$ matrix element. This numerical convergence substantiates the arguments given earlier on the effects that mitigate the need for larger unoccupied spaces for treating the Pauli operator as one goes to heavier nuclei.

We return now to the standard selections made

TABLE III. Comparison of $G^R(\omega)$ in column A with $G(\omega)$ in column B for an analogous s-d shell effective interaction from Ref. 4. In contrast to the results of Table II the Pauli operator plays a relatively minor role here.

$\langle x \mid y \rangle$			
x	y	A	B
$(1d_{5/2})^2$	$(1d_{5/2})^2$	−1.760	−1.836
$(1d_{5/2})^2$	$(2s_{1/2})^2$	−1.591	−0.856
$(1d_{5/2})^2$	$(1d_{3/2})^2$	−3.271	−3.360
$(2s_{1/2})^2$	$(2s_{1/2})^2$	−3.353	−2.510
$(2s_{1/2})^2$	$(1d_{3/2})^2$	−1.299	−0.699
$(1d_{3/2})^2$	$(1d_{3/2})^2$	−0.424	−0.466

for the HFB applications and demonstrate the strong role played by the Pauli operator in this effective interaction. Column A of Table II depicts the reference interaction matrix elements for a part of the submatrix studied in Table I consisting of the first row and the remaining diagonals. We repeat in column B of Table II, for easy reference, the full G matrix elements. The role of the Pauli operator is quite dramatic and underscores our argument that it is preferable to treat it exactly. In Table III, for the sake of contrast, we display from the work of Ref. 4 the more minor role played by the Pauli operator in the effective interaction for light nuclei.

III. HFB THEORY

A. Review of HFB equations

The Hamiltonian is

$$H=\sum_i e_i C_i^\dagger C_i+\frac{1}{4}\sum_{ijkl}\langle ij\,|v_a\,|kl\rangle\, C_i^\dagger C_j^\dagger C_l\, C_k\,, \tag{3.1}$$

where the single-particle energies e_i describe the effect of the core particles on the valence particles $(ijkl)$, and the antisymmetrized effective nucleon-nucleon interaction v_a is derived in Sec. II. Choose the quasiparticle transformations

$$a_i^\dagger=\sum_j (U_{ij}\, C_j^\dagger+V_{ij}\, C_j)\,, \tag{3.2}$$

such that H is approximately characterized by an independent quasiparticle Hamiltonian. That is

$$H'=H-\lambda N=E_0'+\sum_i E_i\, a_i^\dagger a_i+H_{\text{int}}\,, \tag{3.3}$$

where $E_0'+\lambda\langle N\rangle$ is the energy of the quasiparticle vacuum, the E_i are the quasiparticle energies, H_{int} is the neglected quasiparticle interaction involving normal ordered products of four quasiparticle creation or destruction operators, and the chemical potential λ is adjusted so that the

number operator N has the correct expectation value. Requiring the Hamiltonian to have this form results in the HFB equations,[8]

$$\begin{pmatrix} (\mathcal{H}-\lambda) & \Delta \\ -\Delta^* & -(\mathcal{H}-\lambda)^* \end{pmatrix} \begin{pmatrix} U \\ V \end{pmatrix} = E \begin{pmatrix} U \\ V \end{pmatrix} . \tag{3.4}$$

The HF Hamiltonian, the HF potential, and the pair potential are defined by

$$\mathcal{H}_{ij} = (e+\Gamma)_{ij} , \tag{3.5}$$

$$\Gamma_{ij} = \sum_{kl} \langle ik|v_a|jl\rangle \rho_{lk} , \tag{3.6}$$

$$\Delta_{ij} = \frac{1}{2} \sum_{kl} \langle ij|v_a|kl\rangle t_{kl} . \tag{3.7}$$

The density matrix and the pairing tensor are

$$\rho_{ij} = \langle \Phi_0 | C_j^\dagger C_i | \Phi_0 \rangle = (V^\dagger V)_{ij} , \tag{3.8}$$

$$t_{ij} = \langle \Phi_0 | C_j C_i | \Phi_0 \rangle = (V^\dagger U)_{ij} , \tag{3.9}$$

where $|\Phi_0\rangle$ is the quasiparticle vacuum. The HF potential and the pair potential are both constructed with the same effective interaction. No phenomenological pairing force is included. Matrix elements of the interaction between two-particle states $|j_1 j_2 JT\rangle$ of all permissible couplings ($0 \leq J \leq 13$ for our model space) are included in Γ and Δ. The vacuum energy is

$$E_0 = E_{\rm HF} + E_{\rm pair} , \tag{3.10}$$

where

$$E_{\rm HF} = \mathrm{Tr}\left[(e+\tfrac{1}{2}\Gamma)\rho\right], \tag{3.11}$$

$$E_{\rm pair} = \tfrac{1}{2}\,\mathrm{Tr}\,(\Delta t^\dagger). \tag{3.12}$$

The HFB equations (3.4) reduce to the HF equations when Δ and t vanish.

B. Symmetries and canonical representation

Time reversal is a good symmetry for the ground states of even nuclei. Consequently, for each quasiparticle $a_i^\dagger$ there exists a quasiparticle $a_{\bar{i}}^\dagger \equiv T a_i^\dagger T^{-1}$. We choose

$$a_i^\dagger = \sum_k (U_{ik} C_k^\dagger - V_{ik} C_{\bar{k}}), \tag{3.13}$$

$$a_{\bar{i}}^\dagger = \sum_k (U_{ik}^* C_{\bar{k}}^\dagger + V_{ik}^* C_k), \tag{3.14}$$

where $|k\rangle$ denotes $|nljm\tau\rangle$ and is restricted to states where $m-\frac{1}{2}$ is an even integer, and $|\bar{k}\rangle \equiv T|k\rangle$.

The density matrix (3.8) and the pairing tensor (3.9) are represented in the $|k\bar{k}\rangle$ basis by

$$\rho = \begin{pmatrix} (V^\dagger V)^* & 0 \\ 0 & (V^\dagger V) \end{pmatrix} \equiv \begin{pmatrix} \rho_1 & 0 \\ 0 & \rho_1^* \end{pmatrix}, \tag{3.15}$$

$$t = \begin{pmatrix} 0 & (V^\dagger U)^* \\ -(V^\dagger U) & 0 \end{pmatrix} \equiv \begin{pmatrix} 0 & t_1 \\ -t_1^* & 0 \end{pmatrix}. \tag{3.16}$$

Clearly ρ_1 is Hermitian. From (3.9) it is apparent that t is antisymmetric. It therefore follows from (3.16) that t_1 is a Hermitian matrix.

The HFB unitarity constraints[8] are

$$\rho - \rho^2 = tt^\dagger , \tag{3.17}$$

$$\rho t = t\tilde{\rho} . \tag{3.18}$$

Substituting (3.15) and (3.16) into (3.17) and (3.18), we obtain

$$\rho_1 - \rho_1^{\,2} = t_1^{\,2} , \tag{3.19}$$

$$(\rho_1, t_1) = 0 . \tag{3.20}$$

Since the matrices ρ_1 and t_1 are Hermitian and commute, they can be diagonalized by the same unitary transformation. That is, there exists a basis $|\alpha\bar{\alpha}\rangle$, where

$$C_\alpha^\dagger = \sum_k D_{\alpha k} C_k^\dagger , \tag{3.21}$$

$$C_{\bar{\alpha}}^\dagger = \sum_k D_{\alpha k}^* C_{\bar{k}}^\dagger , \tag{3.22}$$

such that ρ and t have the canonical form depicted in Fig. 1. Since ρ_1 and t_1 are Hermitian, the eigenvalues $\rho_{\alpha\alpha}$ and $t_{\alpha\bar{\alpha}}$ are real. From (3.19) it follows that

$$|t_{\alpha\bar{\alpha}}| = [\rho_{\alpha\alpha}(1-\rho_{\alpha\alpha})]^{1/2} . \tag{3.23}$$

It is apparent from Fig. 1 and (3.23) that the HFB quasiparticle vacuum $|\Phi_0\rangle$ represented by (ρ, t) may be expressed in the BCS form

$$|\Phi_0\rangle = \prod_\alpha (u_\alpha + v_\alpha C_\alpha^\dagger C_{\bar{\alpha}}^\dagger)|0\rangle , \tag{3.24}$$

where $\rho_{\alpha\alpha} = v_\alpha^{\,2}$, $t_{\alpha\bar{\alpha}} = u_\alpha v_\alpha$, and u_α and v_α are real.

The canonical representation is extremely useful in the interpretation of HFB wave functions. It does not, however, simplify the calculations, since for a realistic interaction neither the HF Hamiltonian nor the pair potential Δ are diagonalized by the canonical single-particle basis.

All calculations in this paper concerning nuclear ground states use the following symmetries: time reversal; parity; isospin; rotation by π about the x, y, and z axes; and reflection through the xy, yz, and xz planes. Inclusion of this set of symmetries requires that U, V, and D be real. Almost all of our calculations apply axial symmetry about the z axis.

Spherical HFB calculations are presented in Sec. V. Since the valence space does not permit radial mixing, the HF and the pair potentials are

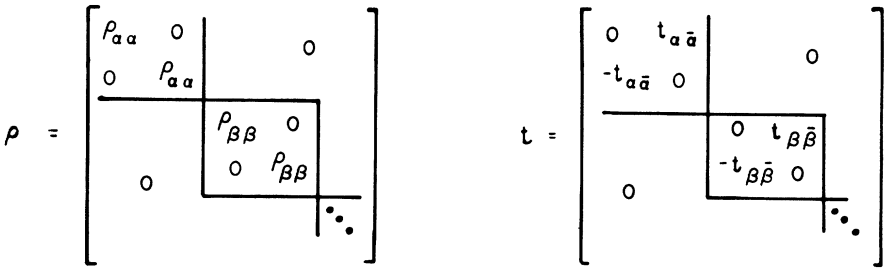

FIG. 1. Canonical representation of the density matrix ρ and the pairing tensor t.

both diagonal in the $|nljm\tau\rangle$ basis. With spherical symmetry and no radial mixing, the HFB equations reduce to the BCS equations

$$\epsilon_{j\tau} = e_{j\tau} + (2j+1)^{-1} \sum_{j'\tau'} v^2_{j'\tau'} \sum_J (2J+1) \langle j\tau j'\tau' J | v_a | j\tau j'\tau' J \rangle , \tag{3.25}$$

$$\Delta_{j\tau} = \tfrac{1}{2} (2j+1)^{-1/2} \sum_{j'\epsilon\tau} (-1)^{l+l'} (2j'+1)^{1/2} \langle j^2 J=0 T=1 | v_a | j'^2 J=0 T=1 \rangle u_{j'\tau} v_{j'\tau} , \tag{3.26}$$

where $|j\rangle$ implies $|nlj\rangle$ and $|\tau\rangle$ is $|p\rangle$ or $|n\rangle$.

IV. DEFORMED RARE-EARTH NUCLEI

A. Model space

An inert core is assumed which contains 40 protons ($1s_{1/2}$ through $2p_{1/2}$) and 70 neutrons ($1s_{1/2}$ through $2d_{3/2}$). The remaining nucleons are in the active valence space which consists of essentially one major oscillator shell of each parity for both neutrons and protons. The active orbitals are listed in Table IV. The maximum number of valence nucleons is 52 protons and 66 neutrons. Since there is no radial mixing, this model space permits angular self-consistency, but not radial self-consistency. The oscillator parameter is $b = (\hbar/m\Omega)^{1/2} = (5.506)^{1/2}$ fm.

Our model space is identical to that used by Banerjee, Mang, and Ring.[9] This will facilitate future direct comparison with their high spin calculations, which utilize the phenomenological pairing plus quadrupole force.

B. Core single-particle energies

The inert core creates a spherical single-particle potential which acts upon the valence particles. This potential is represented by the energies $e_{nlj\tau}$.

A function of this article is to obtain reasonable ground state descriptions of rare-earth nuclei to provide a base for high spin calculations. The core energies play a crucial role in determining the sequence of deformed single-particle levels. This sequence can seriously affect the nature of high spin anomalies. Consequently, considerable care must be exercised in the selection of the core single-particle energies.

The method adopted in this article is to identify spherical HF single-particle energies with spherical Nilsson energies.[10] That is, define $e_{j\tau}$ by

$$\epsilon_{j\tau}(\mathrm{HF}, {}^A Z, \beta_2 = 0) \equiv e_{j\tau}({}^A Z) + \Gamma_{j\tau}({}^A Z, \beta_2 = 0)$$
$$= \epsilon_{j\tau}(\mathrm{Nilsson}, \beta_2 = 0) , \tag{4.1}$$

where Γ is taken from a HF calculation. The Nilsson energies do not depend on mass, except for the trivial $A^{1/3}$ scale factor. The HF potential is a function of ${}^A Z$, with different level orderings for different nuclei. The core energies, as defined by (4.1), are therefore mass dependent.

It is desirable to have a single set of core energies which is suitable for all deformed nuclei studied in this article, that is from ^{154}Gd to ^{178}Os. We define an average energy $\bar{e}$ as follows: For

TABLE IV. Valence space. The active orbitals are listed. The average core energies $\bar{e}$ are defined by (4.3).

Protons		Neutrons	
nlj	$\bar{e}_{nlj}$ (MeV)	nlj	$\bar{e}_{nlj}$ (MeV)
$1h_{9/2}$	19.006	$2g_{9/2}$	12.551
$3s_{1/2}$	11.594	$3p_{1/2}$	11.637
$2d_{3/2}$	14.317	$2f_{5/2}$	13.279
$1h_{11/2}$	11.589	$3p_{3/2}$	9.334
$2d_{5/2}$	9.959	$1i_{13/2}$	10.287
$1g_{7/2}$	14.204	$1h_{9/2}$	15.067
$1g_{9/2}$	7.813	$2f_{7/2}$	7.968
		$1h_{11/2}$	7.543

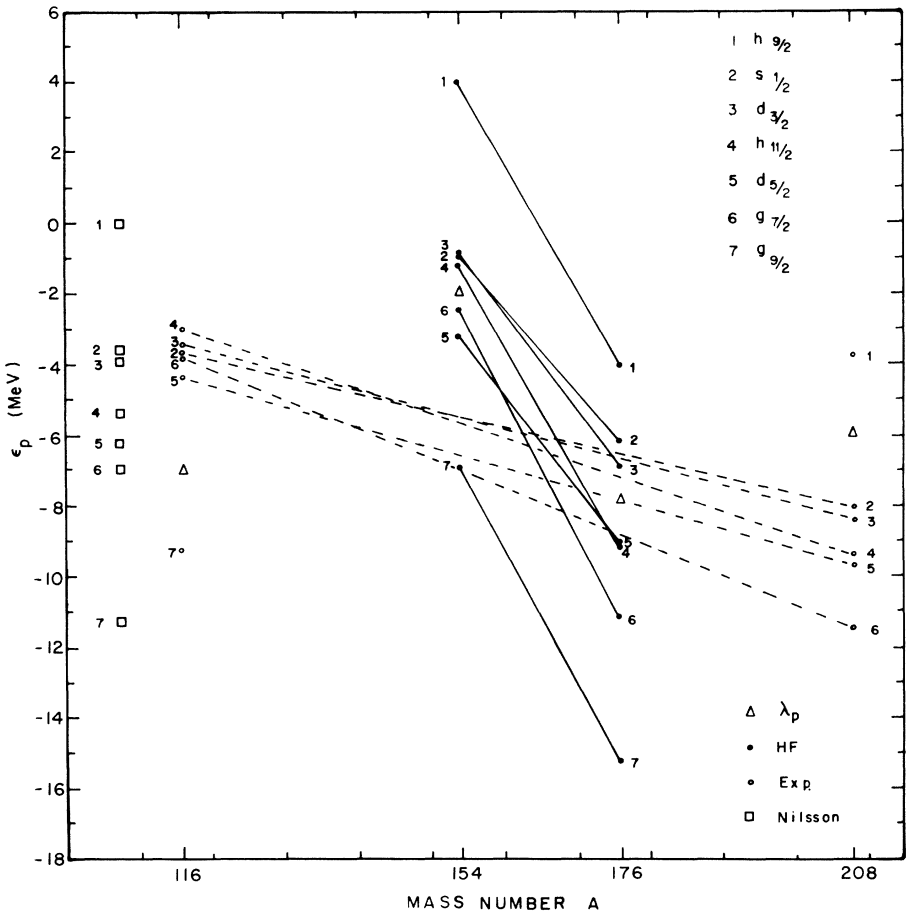

FIG. 2. Proton spherical single-particle energies. The spherical HF spectra of ^{154}Gd and ^{176}Os are compared with the spherical Nilsson energies (Ref. 10) and to the experimental binding energies of a proton relative to ^{208}Pb and ^{116}Sn. The energies relative to ^{208}Pb are deduced from the spectra (Ref. 12) of ^{209}Bi and ^{207}Tl and the proton separation energies (Ref. 13) of ^{209}Bi and ^{208}Pb. The energies relative to ^{116}Sn are deduced from the spectra of ^{117}Sb (Ref. 14) and ^{115}In (Ref. 15) and the proton separation energies (Ref. 13) of ^{117}Sb and ^{116}Sn. The proton Fermi surface λ_p is indicated.

the Nilsson level sequence, ^{154}Gd has a spherical HF potential with the proton subshells ($g_{9/2}, g_{7/2}, d_{5/2}$) and the neutron subshells ($h_{11/2}, f_{7/2}$) fully occupied. Similarly ^{176}Os has a spherical HF potential with the proton levels ($g_{9/2}, g_{7/2}, d_{5/2}, h_{11/2}$) and the neutron levels ($h_{11/2}, f_{7/2}, h_{9/2}$) completely occupied. Define an average spherical HF potential for this mass region by

$$\bar{\Gamma}_{j\tau}(\beta_2=0)=\tfrac{1}{2}[\Gamma_{j\tau}(^{154}\mathrm{Gd},\beta_2=0)+\Gamma_{j\tau}(^{176}\mathrm{Os},\beta_2=0)]\,. \tag{4.2}$$

The average core energies are then defined by

$$\bar{e}_{j\tau}+\bar{\Gamma}_{j\tau}(\beta_2=0)=\epsilon_{j\tau}(\mathrm{Nilsson},\beta_2=0)\,. \tag{4.3}$$

where the well tested Nilsson energies are evaluated for the average mass $A=166$. Table IV lists $\bar{e}_{j\tau}$.

How reasonable is this set of average energies? The spherical HF spectra of ^{154}Gd and ^{176}Os obtained with $\bar{e}$ are presented in Fig. 2 and Fig. 3. The sets of occupied levels are preserved. That is, there are no level crossings through the Fermi surface when $e(^AZ)$ is replaced by $\bar{e}$. Experimental proton single-particle energies are given for ^{116}Sn and ^{208}Pb. The experimental neutron energies are depicted for ^{140}Ce and ^{208}Pb. Notice that both the experimental and the HF level sequences are mass dependent. There is considerable similarity between the experimental and the theoretical level crossings. The neutron pair ($h_{9/2}, f_{7/2}$) and the proton pairs ($d_{5/2}, g_{7/2}$) and ($s_{1/2}, d_{3/2}$) cross. Also the high j orbits have a greater mass dependence than the low j orbits. These observations indicate that the effective interaction is reproducing some fine details in the mass dependence of the experi-

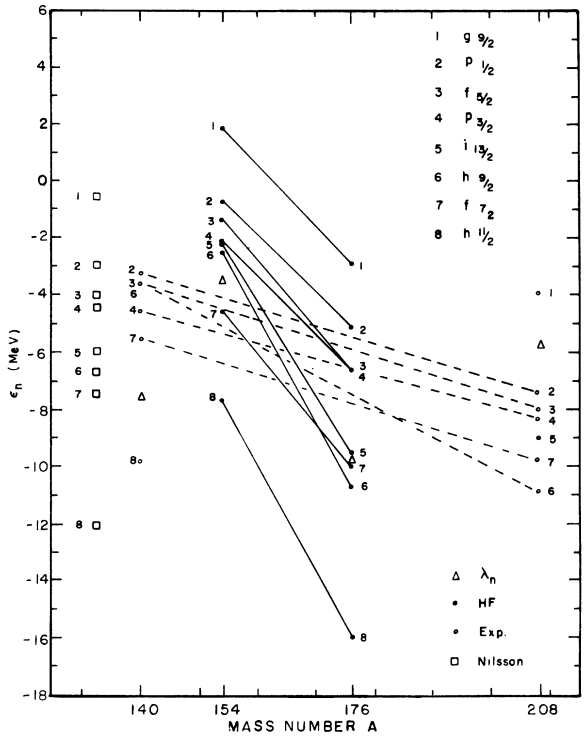

FIG. 3. Neutron spherical single-particle energies. The spherical HF spectra of ^{154}Gd and ^{176}Os are compared with the spherical Nilsson energies (Ref. 10) and to the binding energies of a neutron relative to ^{208}Pb and ^{140}Ce. The energies relative to ^{208}Pb are deduced from the spectra (Ref. 12) of ^{209}Pb and ^{207}Pb and the neutron separation energies (Ref. 13) of ^{209}Pb and ^{208}Pb. The energies relative to ^{140}Ce are deduced from the spectra (Ref. 16) of ^{141}Ce and ^{139}Ce and the neutron separation energies (Ref. 13) of ^{141}Ce and ^{140}Ce. The neutron Fermi surface λ_n is indicated.

mental single-particle energies. The Nilsson energies are also displayed in Fig. 2 and Fig. 3. Notice that each Nilsson energy equals the midpoint of the corresponding HF line. We hope that this choice of a single set of average core energies will not only retain the advantages of the tested Nilsson energies, but will also permit the effective interaction to introduce mass dependent level crossings.

C. HF with quadrupole constraint

Light nuclei exhibit a large number of solutions to self-consistent field equations. For instance with the Rosenfeld interaction ^{24}Mg has three prolate, three oblate, and at least one nonaxial HF solutions.[17] With the Yale interaction ^{24}Mg has three nonaxial HF states.[18] Most rare-earth studies use the pairing plus quadrupole interaction[2,11] and report only one prolate shape. A realistic interaction might produce a more convoluted energy surface, and hence more minima.

To test this possibility HF studies with an external quadrupole constraint[19] have been performed. Replace H by

$$H' = H - \chi Q_{20}, \tag{4.4}$$

where Q_{20} is the mass quadrupole operator and χ is a Lagrange multiplier which can be adjusted so that Q_{20} has the desired expectation value. The HFB equations (3.4) reduce to the HF equations when $\Delta = 0$. To include the quadrupole term $\mathcal{K}$ is simply replaced by $\mathcal{K} - \chi Q_{20}$. This technique serves two functions. First, it partially maps out the energy surface as a function of deformation. Second, it assists in the search for new minima.

The deformation and binding energy of ^{168}Yb for prolate axial shapes are presented in Fig. 4 as a function of χ. There are three branches. Each branch begins and ends when either the neutron or the proton HF gap vanishes. Decreasing χ at the left end of a branch or increasing χ at the right end produces a level crossing at the Fermi

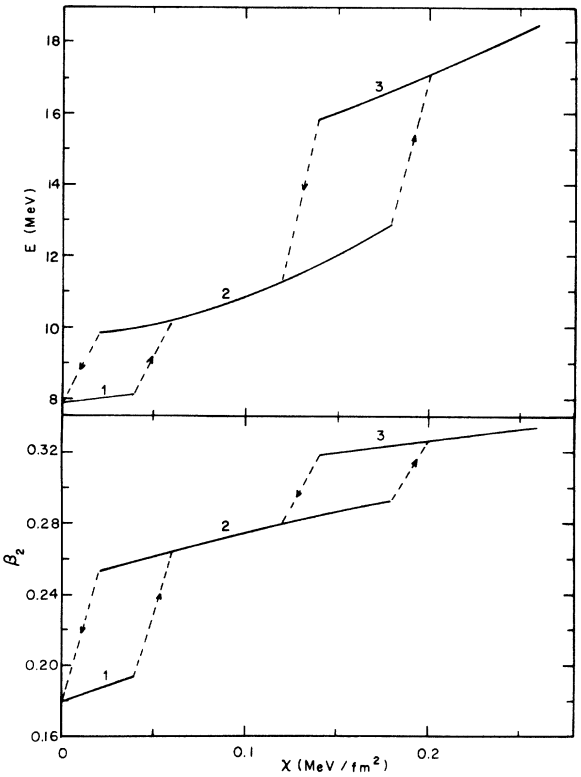

FIG. 4. The deformation β_2 and the energy E as a function of the quadrupole Lagrange multiplier χ. These constrained HF curves are for ^{168}Yb. The dotted lines indicate discontinuous jumps from one branch to another. The numbers on the β_2 and E curves correspond to each other.

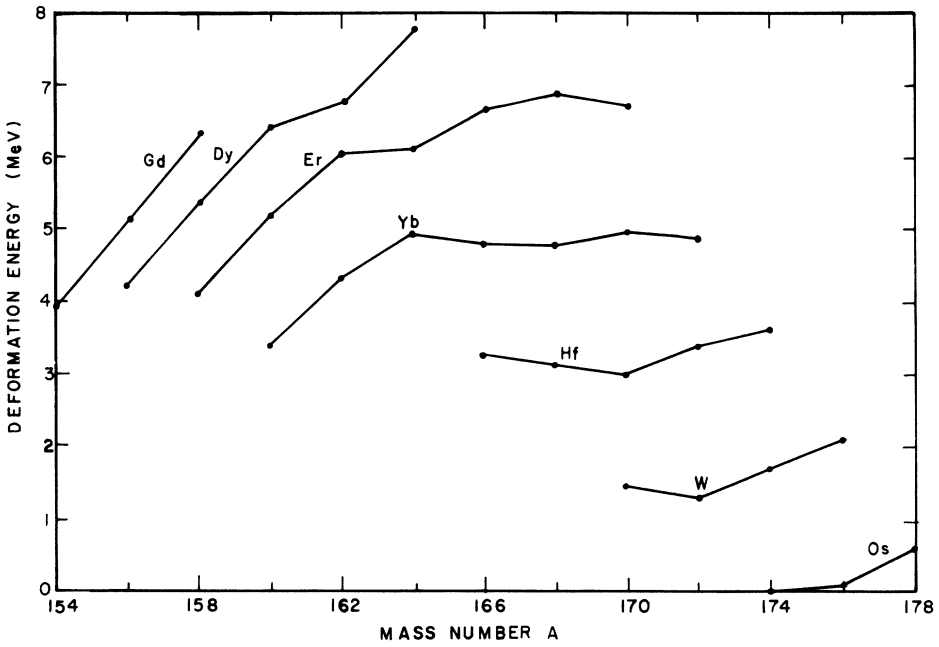

FIG. 5. The deformation energy is the difference in energy between the spherical HFB state and the lowest deformed HFB state.

surface. In HF theory this creates a discontinuous change in the set of occupied orbits, and hence discontinuities in properties of the wave function, such as deformation and binding energy. The significant feature of Fig. 4 is that the higher branches (2, 3) do not extend back to $\chi = 0$. Hence for the Hamiltonian H there appears to be only one prolate axial solution to the HF equations for ^{168}Yb. Of course one can never claim with certainty that since other solutions have not been discovered, therefore they do not exist.

D. Deformation energies

What are the ground state shapes of rare-earth nuclei ($N = 82-126$, $Z = 50-82$)? There have been two theoretical methods for calculating deformations: the Nilsson model[10,20,29] and the pairing plus quadrupole model[2,11,29]. They find that nuclei near the magic numbers $N = 82$ and $Z = 50$ are spherical. There is a transition region at $N = 86-90$ in which the lowest minimum suddenly changes from spherical to prolate. Around $A = 190$ the deformations gradually alter from prolate to oblate. The shapes again become spherical near ^{208}Pb. Very few rare-earth nuclei are predicted to be axially asymmetric.

In our studies, the possibility of nonaxial ground states is tested in the context of high spin calculations[21] using the cranking model, which replaces H by $H - \omega J_x$. For excited states ($\omega \neq 0$), the intrinsic shape must be nonaxial. These nonaxial HFB wave functions can be used as trial wave functions for ground state ($\omega = 0$) HFB calculations. If the final self-consistent shape is axial for $\omega = 0$, this indicates that the axial solution is stable against nonaxial perturbations and suggests that the ground state is indeed axially symmetric. This procedure has been performed for ^{168,170,172}Yb and ^{174}Hf. In all cases the nonaxial shapes obtained when $\omega \neq 0$ are restored to axiality when ω is reduced to zero. Consequently, we may conclude that the ground states of these nuclei are indeed axial. The studies which follow are restricted to axial shapes.

Ground state properties have been calculated for 35 even nuclei with $Z = 64-76$ and $N = 90-102$. The deformation energy E_{def} is defined as the difference in energy between the spherical HFB state and the lowest deformed HFB state. Figure 5 displays E_{def} as a function of A. As N increases from 90, E_{def} increases rapidly for each Z. The deformation energy is largest around $N = 100$, which is near the middle of the neutron shell. The midpoint of the proton shell is $_{66}$Dy. Accordingly the systematic relations

$$E_{\text{def}}(N, Z) < E_{\text{def}}(N, Z+2) \quad (Z < 66), \tag{4.5}$$

$$E_{\text{def}}(N, Z) > E_{\text{def}}(N, Z+2) \quad (Z \geq 66) \tag{4.6}$$

are observed for all N. For $Z \geq 72$, the deformation energy rapidly decreases. The Os isotopes

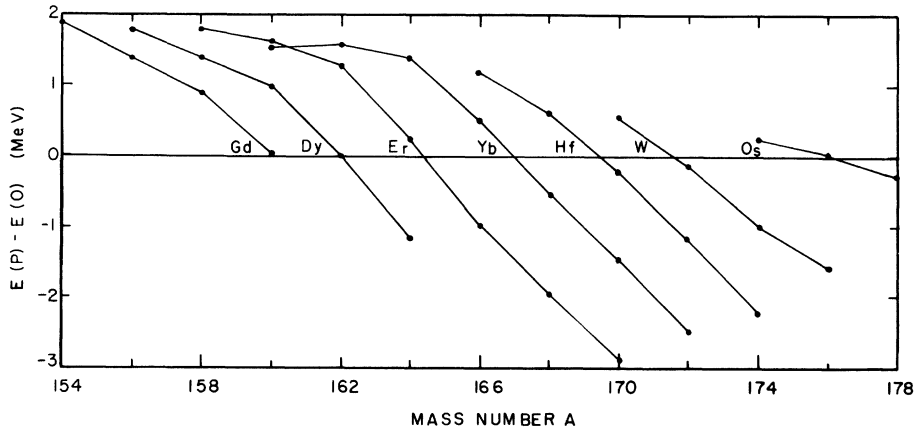

FIG. 6. The energy difference between prolate and oblate HFB solutions. Negative differences correspond to prolate ground states.

are predicted to be extremely soft. These results are in general agreement with Kumar and Baranger[2] and with Gotz, Pauli, and Alder.[20]

The difference in energy between the prolate and oblate HFB states, $E_{PO}=E(P)-E(O)$, is presented in Fig. 6. With the exception of ^{174,176}Os, nuclei with $N \leq 96$ are oblate, whereas those with $N \geq 96$ are prolate. This is in disagreement with Refs. 2 and 20, which predict all of these nuclei to be prolate. Experimentally the sign of the quadrupole deformation of an even nucleus is usually not directly measured, but is deduced from the sign of adjacent odd nuclei. However, such observables as moments of inertia, odd-even mass differences, and the magnitudes of the quadrupole deformation vary in such a smooth manner with the mass number in this region that it appears unlikely that there really is a shape transition from oblate to prolate at $N=96$.

The energy difference E_{PO} decreases rapidly as N increases. Also E_{PO} increases slowly with Z. Notice that at $N=90$ these curves are becoming horizontal. The N, Z systematics of the E_{PO} curves are in accord with previous investigations.[2,20] What is required for complete agreement is a uniform downward shift of all curves by a few MeV, so that all nuclei would be prolate. There are two possible sources of this discrepancy. First is the effective interaction, and second is the single-particle energies of the core.

The effective interaction is a bare G matrix. An improved effective interaction would include contributions due to polarization of the inert core. These renormalization terms have been calculated for light nuclei,[22] and they are remarkably correlated with the matrix elements of the quadrupole-quadrupole interaction.[11] Moreover, it is well established that the quadrupole-quadrupole force favors prolate shapes in this mass region.[2] So it is possible that inclusion of these corrections to the effective interaction would favor prolate shapes and resolve this discrepancy. Unfortunately, for heavy nuclei, core polarization terms are exceedingly difficult to calculate.

Part of the solution may lie in the determination of the G matrix itself. It was calculated in a two-particle basis of good isospin T. This means that neutrons and protons have the same oscillator length b in their radial wave functions. Consequently, neutrons filling oscillator shell $N=6$ have an rms radius 8% greater than protons filling oscillator shell $N=5$. However, it is known from experiment that neutrons and protons differ by only a few percent in their radii. Therefore neutrons and protons must have different oscillator parameters ($b_n \neq b_p$). Assume that the effective interaction is inversely proportional to the volume, then $v \propto 1/R_{\text{rms}}{}^3$. If R_{rms} for neutrons is too large by 8% then the neutron-neutron interaction v_{nn} could be too weak by 25%.

The possible consequences of this error have been crudely estimated by a simple scaling of the interaction. That is v_{nn} is increased by 20%, v_{np} by 10%, while v_{pp} is unaltered. This scaled interaction is used only in the present discussion, and nowhere else unless explicitly mentioned. The E_{PO} curve for Er using this scaled force is given in Fig. 7. The shape of the curve is the same as for the original interaction (Fig. 6), but it is shifted downwards by 1.1 MeV. The deformation of ^{164}Er is changed from oblate to prolate. Consequently, using separate oscillator lengths for neutrons and protons may favor prolate over oblate shapes.

The prolate-oblate energy difference may also depend upon the choice of core single-particle

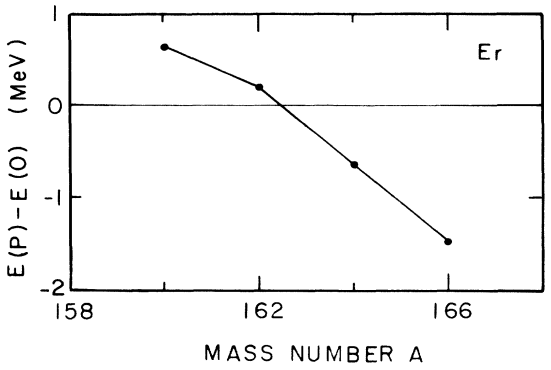

FIG. 7. The energy difference between prolate and oblate HFB states for Er. The scaled interaction described in Sec. IV D is used. See Fig. 6.

energies. Consider a change in e such that the average spherical HF single-particle energies are uniformly compressed or expanded. That is

$$\bar{e}_{j\tau}(s)+\bar{\Gamma}_{j\tau}(\beta_2=0)=s\epsilon_{j\tau}(\text{Nilsson},\beta_2=0)\,, \quad (4.7)$$

where $\bar{\Gamma}$ is defined by (4.2) and s is a scale factor. In Fig. 8 E_{PO} is presented for ^{162}Er for $s=1.0$, 0.9, and 0.8. Compressing the HF spectrum by 20% ($s=0.8$) lowers the prolate shape relative to the oblate shape by 0.9 MeV, but the nucleus remains oblate. The same comparison is made with the scaled interaction discussed above. In this case, compressing the spectrum favors the oblate shape. The core energies may be adjusted so that the spectra of near magic odd nuclei for $Z=50$, 82 and $N=82$, 126 are reproduced by spherical HFB quasiparticle spectra. Modest shifts of $\bar{e}$ accomplish this. Figure 8 also gives E_{PO} for these shifted core energies. Unfortunately, they do not favor the prolate shape.

Finally, we can shift e for one $j\tau$, holding all other fixed. HF calculations were performed for ^{162}Er moving the $i_{13/2}$, $g_{7/2}$, and $d_{5/2}$ levels by ± 0.2 MeV. There was no appreciable change in E_{PO}. Larger shifts of a single level would adversely alter the sequence of deformed single-particle states. Throughout the remainder of this section we use the original average core energies defined by (4.3) and listed in Table IV.

The prediction of oblate shapes for $N \leq 96$ is a serious deficiency of our Hamiltonian. Probable sources of error have been discussed above, and we hope that future improvements will rectify this difficulty.

The characteristics of the prolate HFB states will now be analyzed in detail. The mass dependence of deformation parameters, pair gaps, and two-particle separation energies are reviewed. The deformed single-particle level sequence will also be discussed.

E. Deformations

The shape of an intrinsic state can be characterized by its multipole moments

$$Q_{\text{LM}}=\left\langle \sum_i r_i^L\, Y_{\text{LM}}(\Omega_i)\right\rangle, \quad (4.8)$$

and by its radial moments

$$R_L=\left\langle \sum_i r_i^L\right\rangle, \quad (4.9)$$

where the sums are on the active valence nucleons. If the shapes are axially symmetric, then the deformation parameters β_L have the simple form

$$\beta_L=\frac{4\pi}{L+3}\,\frac{Q_{L0}}{R_L}\,. \quad (4.10)$$

The quadrupole deformation β_2 is presented in Fig. 9. For both HFB and experiment all nuclei obey the rules

$$\beta_2(N,Z)>\beta_2(N,Z+2)\,, \quad (4.11)$$

$$\beta_2(A,Z)>\beta_2(A,Z+2)\,. \quad (4.12)$$

The systematic behavior characterized by Eq.

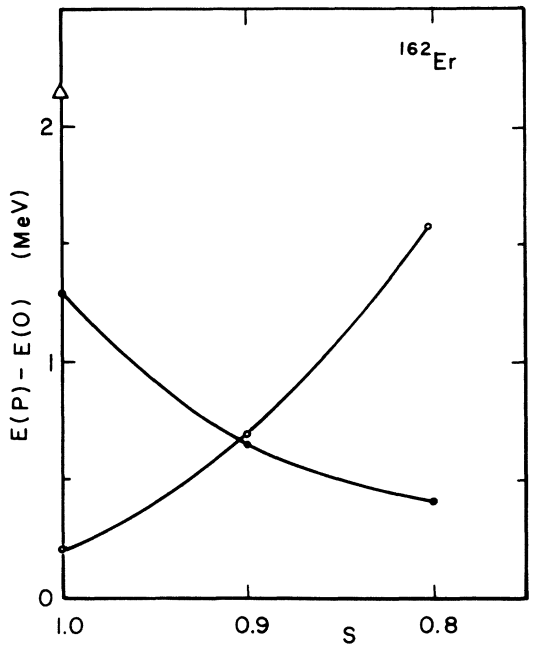

FIG. 8. The energy difference between prolate and oblate HFB states for ^{162}Er as a function of the HF spectrum scale factor defined in (4.7). The solid circles are for the original interaction. The open circles correspond to the scaled interaction described in Sec. IV D. The triangle denotes the core energies designed for spherical near magic nuclei. See Fig. 6.

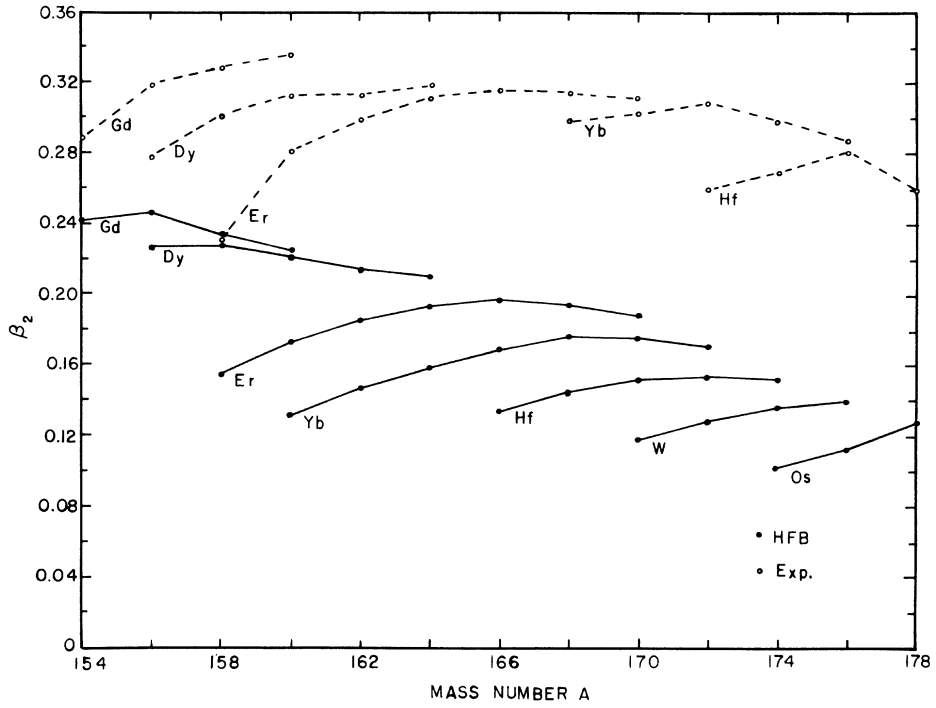

FIG. 9. The quadrupole deformation β_2. Experimental values are from Ref. 23.

(4.11) is understood by noting that the proton shell $Z = 50-82$ has the midpoint ${}_{66}$Dy. For $Z > 66$ the nuclei are moving from an open proton shell region towards a closed proton shell region. Hence the deformation β_2 should decrease as Z increases. Similarly, the midpoint of the neutron shell $N = 82-126$ is $N = 104$. The 35 even nuclei included in Fig. 9 range from $N = 90$ to $N = 102$. Therefore they are moving from a closed neutron shell region towards an open shell region. Consequently, adding two neutrons should increase the deformation. This explains Eq. (4.12), which states that adding two protons and subtracting two neutrons decreases β_2. Each of the isotopic curves peak in the vicinity of $N = 100$. The maxima of the theoretical and experimental curves lie within a few neutrons of one another. We may conclude that the N, Z systematics of β_2 agree fairly well with experiment.

The magnitudes of β_2 are too small. This is probably due to several factors. First, the polarization of the inert core has been omitted in the calculation of the effective interaction. These renormalization terms may resemble a quadrupole-quadrupole interaction, and would then increase β_2. Second, the G matrix has been calculated with the same oscillator length for neutrons and protons ($b_n = b_p$). It has been argued in Sec. IV D that this probably underestimates the effective neutron-neutron interaction by ~25%. Scaling the force by increasing v_{nn} by 20%, v_{np} by 10%, and leaving v_{pp} unchanged increases $\beta_2(^{162}\mathrm{Er})$ from 0.186 to 0.239. The experimental value is 0.299. Third, the valence space is limited to one oscillator shell for each parity for both protons and neutrons. It has been demonstrated that extending the valence space to higher shells can increase β_2 by as much as 40%.[24] These three effects probably account for the small magnitudes of β_2.

The hexadecapole deformation β_4 is shown in Fig. 10. The essential feature is that for both theory and experiment there is a smooth transition from positive β_4 to negative β_4 near $A = 170$. This characteristic is also predicted by Nilsson calculations[20,28] and by HF calculations with the Skyrme interaction.[29] Since the experimental errors[25-27] range from ±0.03 to ±0.05, the theoretical magnitudes are in accord with experiment. The HFB magnitudes are quite similar to the Nilsson and Skyrme values.

F. Pairing gaps

The pair field (3.7) is calculated with the same effective interaction as is used to construct the HF potential (3.6). In the canonical representation described in Sec. III B, the pair field is

$$\Delta_{\alpha\bar{\alpha}'} = \sum_{\beta} \langle \alpha\bar{\alpha}' | v_a | \beta\bar{\beta} \rangle u_\beta v_\beta . \tag{4.13}$$

It should be noted that $\Delta_{\alpha\bar{\alpha}'}$ does not vanish when

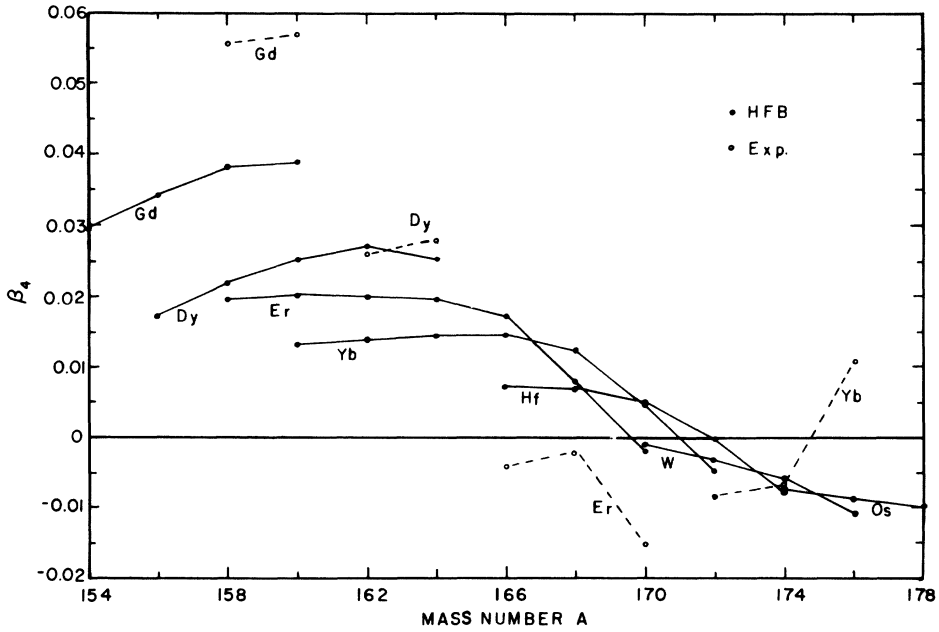

FIG. 10. The hexadecapole deformation β_4. Experimental values are from Ref. 27, except for Yb which are from Ref. 26.

$\alpha \neq \alpha'$. Furthermore, the pair field is state dependent, since for each pair of single-particle orbits $|\alpha\bar{\alpha}\rangle$ there is a different pairing gap $\Delta_{\alpha\bar{\alpha}}$. The average pairing gap may be defined as

$$\bar{\Delta}=\frac{1}{m}\sum_{\alpha=1}^{m}\Delta_{\alpha\bar{\alpha}}, \tag{4.14}$$

where m is the number of pairs of single-particle states. Separate averages $\bar{\Delta}_n$ and $\bar{\Delta}_p$ have been calculated for neutrons and protons.

The average pairing gaps are compared with the experimental odd-even mass differences P_n and P_p. For each even nucleus the mass difference is averaged over adjacent odd nuclei,[30] so that

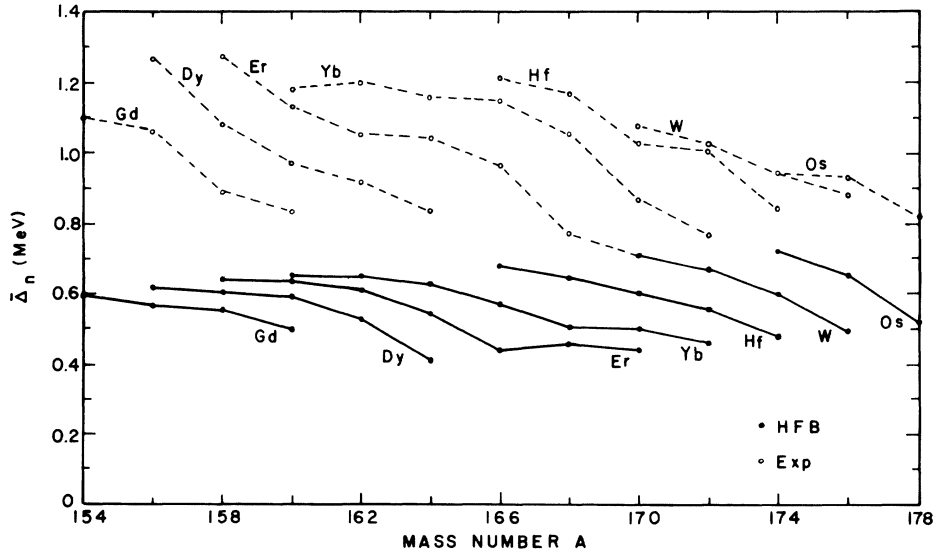

FIG. 11. The average neutron pairing gap. The HFB values of (4.14) are compared with the experimental odd-even mass differences.

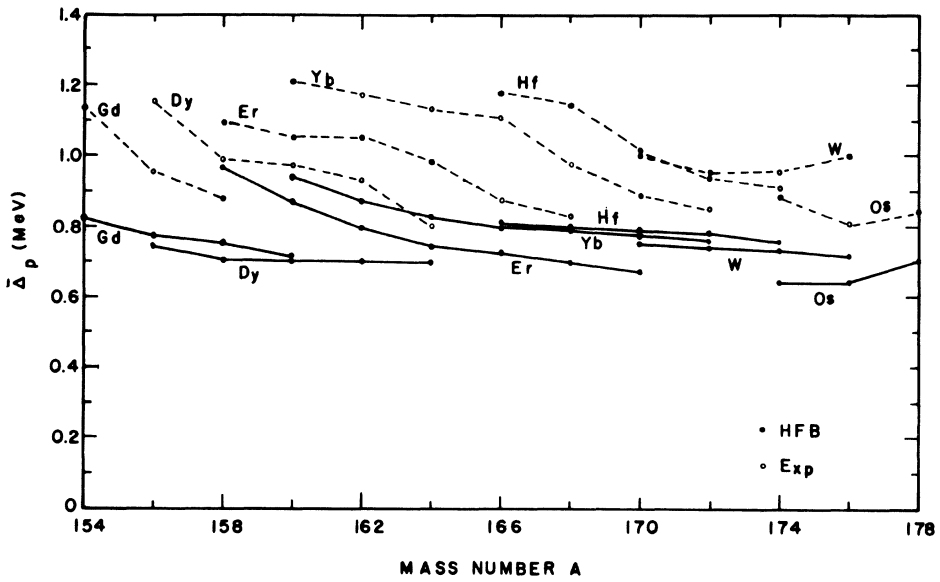

FIG. 12. The average proton pairing gap. See Fig. 11.

$$P_n = \tfrac{1}{4}[2S_n(N,Z) - S_n(N+1,Z) - S_n(N-1,Z)], \tag{4.15}$$

$$P_p = \tfrac{1}{4}[2S_p(N,Z) - S_p(N,Z+1) - S_p(N,Z-1)], \tag{4.16}$$

where the separation energies S_n and S_p are defined by

$$S_n(N,Z) = B(N,Z) - B(N-1,Z), \tag{4.17}$$

$$S_p(N,Z) = B(N,Z) - B(N,Z-1), \tag{4.18}$$

where $B(N,Z)$ is the experimental binding energy. The separation energies are taken from mass tables.[31]

The average neutron pairing gap is shown in Fig. 11. With the exception of ^{166}Er (theory) and ^{160}Yb (exp), all experimental and theoretical curves follow the rule

$$\bar{\Delta}_n(N,Z) > \bar{\Delta}_n(N+2,Z). \tag{4.19}$$

Presumably this is caused by two effects. First, the effective pairing force decreases as the mass increases. Second, since β_2 increases with A and since the valence space spans only two oscillator shells, it follows that the level density decreases as A increases. This reduces the pairing gap.

Another systematic pattern followed by all nuclei, except the experimental values of ^{158}Er, ^{168}Yb, and W, is

$$\bar{\Delta}_n(N,Z) < \bar{\Delta}_n(N,Z+2). \tag{4.20}$$

Perhaps this follows from Eq. (4.11), which states that adding two protons reduces β_2, and therefore increases the level density.

The magnitudes of $\bar{\Delta}_n$ are substantially too small. This is partly caused by choosing $b_n = b_p$, with the resultant underestimate of v_{nn} as has been discussed above. With the scaled interaction (v_{nn} increased by 20%, v_{np} by 10%), the average gap $\bar{\Delta}_n$ of ^{168}Yb is increased from 0.505 to 0.650 MeV. Although the N,Z systematics of the neutron pairing gap are very well reproduced, the small magnitudes constitute a serious defect of the present Hamiltonian.

The average proton pairing gap is presented in Fig. 12. All nuclei, with the exception of W(exp) and Os, display the relation

$$\bar{\Delta}_p(N,Z) > \bar{\Delta}_p(N+2,Z). \tag{4.21}$$

For the mass region being considered adding two neutrons increases β_2 and lowers the level density, which may explain (4.21).

Most Dy, Er, and Yb isotopes follow

$$\bar{\Delta}_p(N,Z) < \bar{\Delta}_p(N,Z+2), \tag{4.22}$$

whereas most Hf and W values are governed by the inverse of (4.22). The N,Z systematics of the proton pairing gap are faithfully reproduced.

The magnitudes of $\bar{\Delta}_p$ are much closer to the odd-even mass differences than are the magnitudes of $\bar{\Delta}_n$. This tends to confirm the suspected relative weakness of the neutron-neutron effective interaction.

G. Two-particle separation energies

The Hamiltonian (3.1) contains relative single-particle energies describing an inert core. Con-

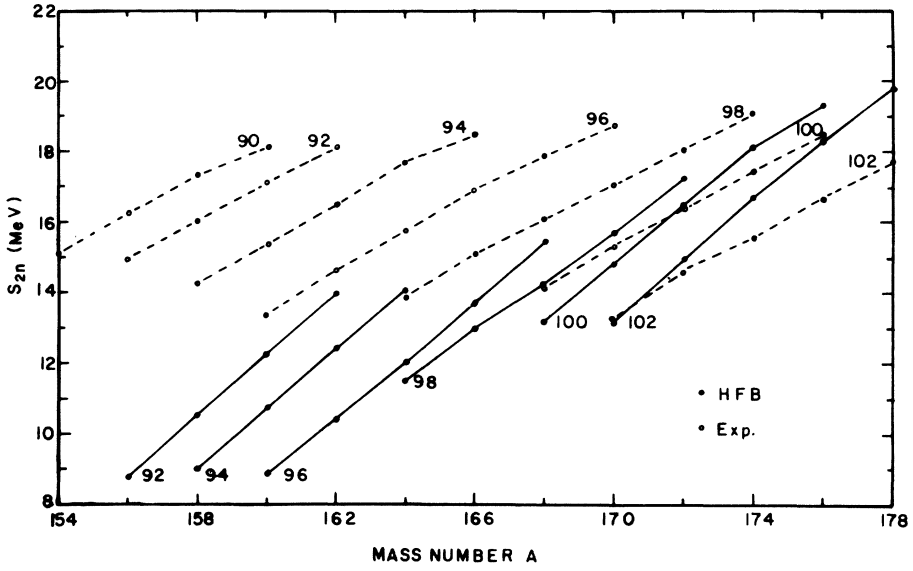

FIG. 13. Separation energy of two neutrons. Isotonic curves are labeled by N. Experimental values are from Ref. 26.

sequently, the resulting binding energies have only relative and not absolute significance. Relative binding energies of even nuclei may be described by the separation energies of two neutrons, S_{2n}, or two protons, S_{2p}. Their definitions may be inferred from (4.17) and (4.18).

We consider the dependence of S_{2n} on the proton number and the dependence of S_{2p} on the neutron number.[32] Graphs of $S_{2n}(Z)$ and $S_{2p}(N)$ are useful for detecting shell structure. Large gaps between adjacent lines indicate the presence of magic numbers. Accordingly, isotonic curves of S_{2n} are presented in Fig. 13, and isotopic curves of S_{2p} are drawn in Fig. 14. All theoretical and experimental points adhere to the Way and Wood relations[33]:

$$S_{2n}(N,Z) < S_{2n}(N,Z+2), \tag{4.23}$$

$$S_{2p}(N,Z) < S_{2p}(N+2,Z), \tag{4.24}$$

which were deduced from β-decay energy systematics. In addition all points follow the rules

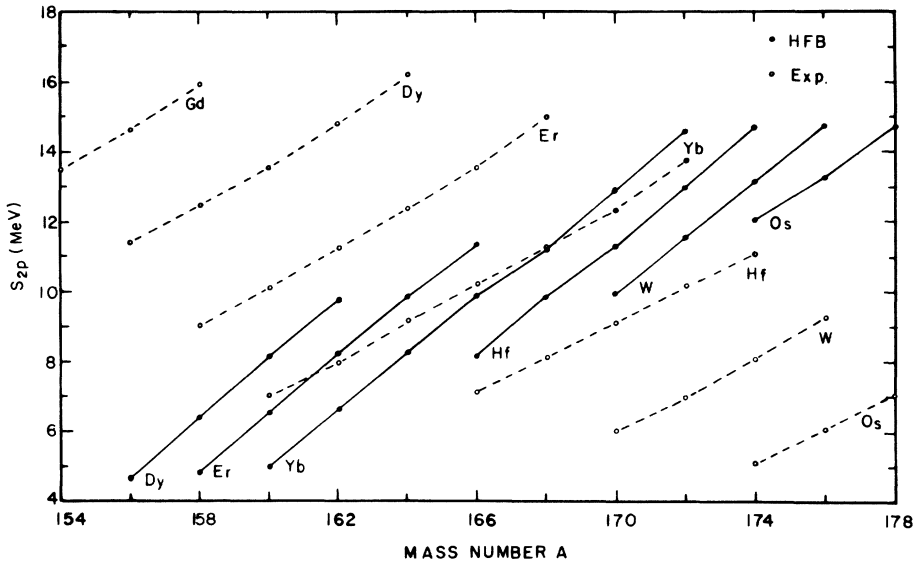

FIG. 14. Separation energy of two protons. Isotopic curves are labeled by Z. Experimental values are from Ref. 31.

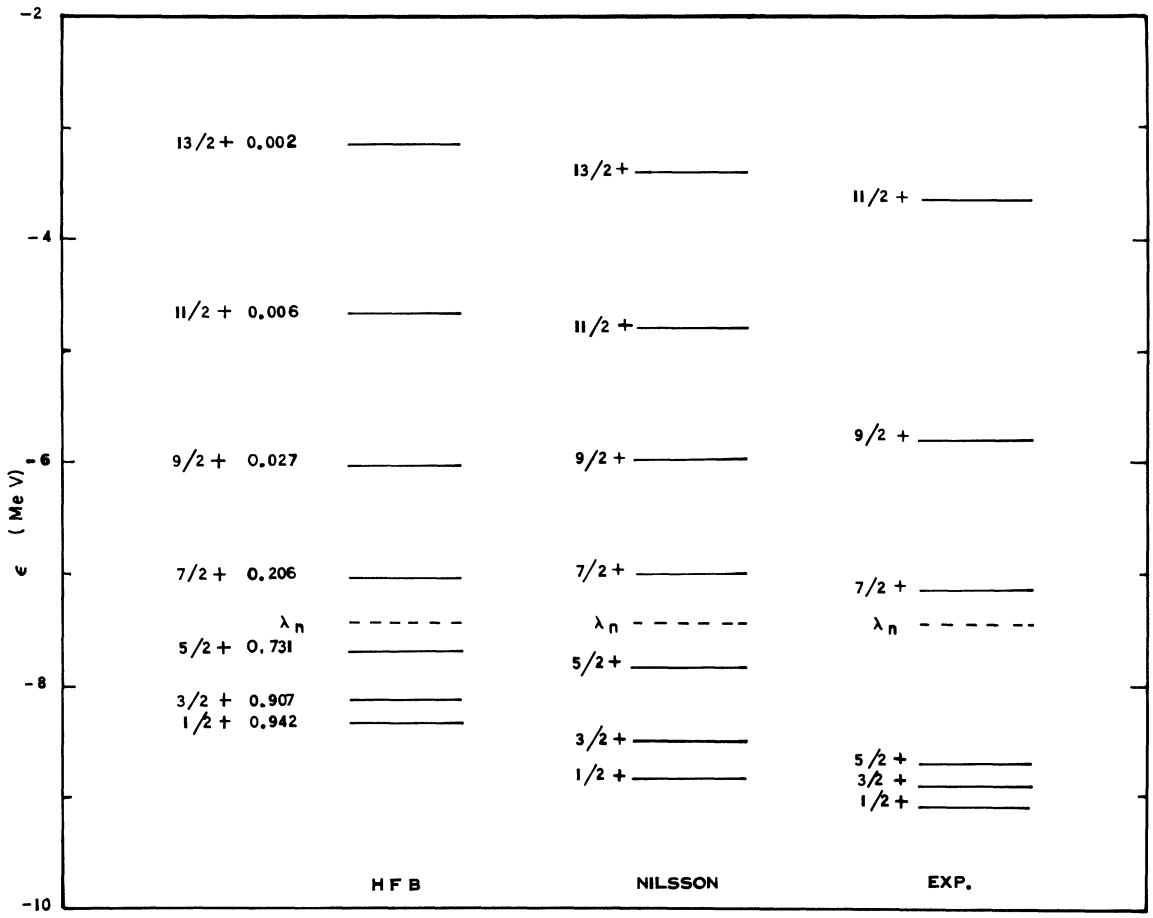

FIG. 15. Deformed single-particle neutron levels which are primarily $i_{13/2}$. The HFB sequence for ^{168}Yb is compared with the Nilsson levels (Ref. 10) for ^{168}Yb and to the experimental levels (Ref. 34) of ^{169}Yb. The angular momentum projection m labels each state. The HFB levels include the occupation probabilities $v_\alpha{}^2$.

$$S_{2n}(A,N) > S_{2n}(A,N+2), \tag{4.25}$$

$$S_{2p}(A,Z) > S_{2p}(A,Z+2). \tag{4.26}$$

The dependence of S_{2n} on the neutron number and the dependence of S_{2p} on the proton number may be inferred from Fig. 13 and Fig. 14. The experimental points are governed by

$$S_{2n}(N,Z) > S_{2n}(N+2,Z), \tag{4.27}$$

$$S_{2p}(N,Z) > S_{2p}(N,Z+2), \tag{4.28}$$

whereas most theoretical values obey the inverses of (4.27) and (4.28).

We may conclude that the theory reproduces the systematic behavior of $S_{2n}(Z)$ and $S_{2p}(N)$ but does not correctly predict $S_{2n}(N)$ and $S_{2p}(Z)$. The binding effect of the interaction over the entire mass region is given by $B(^{178}\mathrm{Os}) - B(^{154}\mathrm{Gd})$. The theoretical value of 144.5 MeV compares favorably with the experimental value[31] of 153.6 MeV.

H. Deformed single-particle levels

The ultimate purpose of this program of studies is to describe high spin states in rare-earth nuclei. The precise nature of backbending mechanisms depends very delicately on the ordering of and intervals between the deformed single-particle levels. The sequence of levels at the neutron Fermi surface is especially significant. Most important of all is the location of the orbits whose primary component is $i_{13/2}$, for it is in this subshell that the inertial forces are the strongest. For a theoretical calculation to have any hopes of a reasonable description of high spin anomalies, the $i_{13/2}$ levels must assume their proper location about the Fermi surface.

In the canonical representation (Sec. III B) the HF Hamiltonian (3.5) is

$$\mathcal{H}_{\alpha\alpha'} = \langle\alpha|\bar{e}|\alpha'\rangle + \sum_\beta \langle\alpha\beta|v_a|\alpha'\beta\rangle v_\beta{}^2. \tag{4.29}$$

The canonical basis $|\alpha\rangle$ does not diagonalize $\mathcal{H}$. The single-particle energies of the canonical orbits are defined by $\epsilon_\alpha = \mathcal{H}_{\alpha\alpha}$. For axially symmetric shapes each level $|\alpha\rangle$ has as a good quantum number m, the projection of the angular momentum on the symmetry axis.

Since the $i_{13/2}$ orbit is far removed from other positive parity subshells, j is approximately conserved for $i_{13/2}$. Consequently, the level sequence of the magnetic substates of $i_{13/2}$ is readily isolated. This sequence for ^{168}Yb is presented in Fig. 15. The Nilsson sequence[10] for ^{168}Yb and $\beta_2 = 0.225$ ($\epsilon = 0.2$) as well as the experimental single-particle energies of ^{169}Yb (Ref. 34) are also presented in Fig. 15. The Nilsson and experimental bands have been shifted so that their Fermi surfaces coincide with λ_n of the HFB band.

The inertial forces are proportional to J_x. The matrix elements of J_x are largest for $m = \frac{1}{2}$ and decrease monotonically as m increases. Since the strength of the inertial forces near the Fermi surface governs the nature of high spin anomalies, the location of λ_n relative to the magnetic substates of $i_{13/2}$ is of great consequence. The significant aspect of Fig. 15 is that for all three bands λ_n lies between the $m = \frac{5}{2}$ and $m = \frac{7}{2}$ levels. This is extremely encouraging and offers hope that high spin calculations commencing from this ground state level sequence will be physically reasonable. Finally, we note that for all three bands, the energy intervals increase as m increases.

V. SPHERICAL SEMIMAGIC NUCLEI

Because of the complexity of the numerical computation the self-consistent calculation is of necessity limited to a modest number of particles, and the core of 40 protons and 70 neutrons must be assumed to simply furnish a set of single-particle spherical core energies. These energies are chosen so that the total one-body field, coming both from the core and from the self-consistent treatment of the two-body force acting among the active particles, agrees with the observed single-particle properties. Once determined, this set of core energies is held fixed for all the calculated nuclei, for all deformations, and all angular momenta.

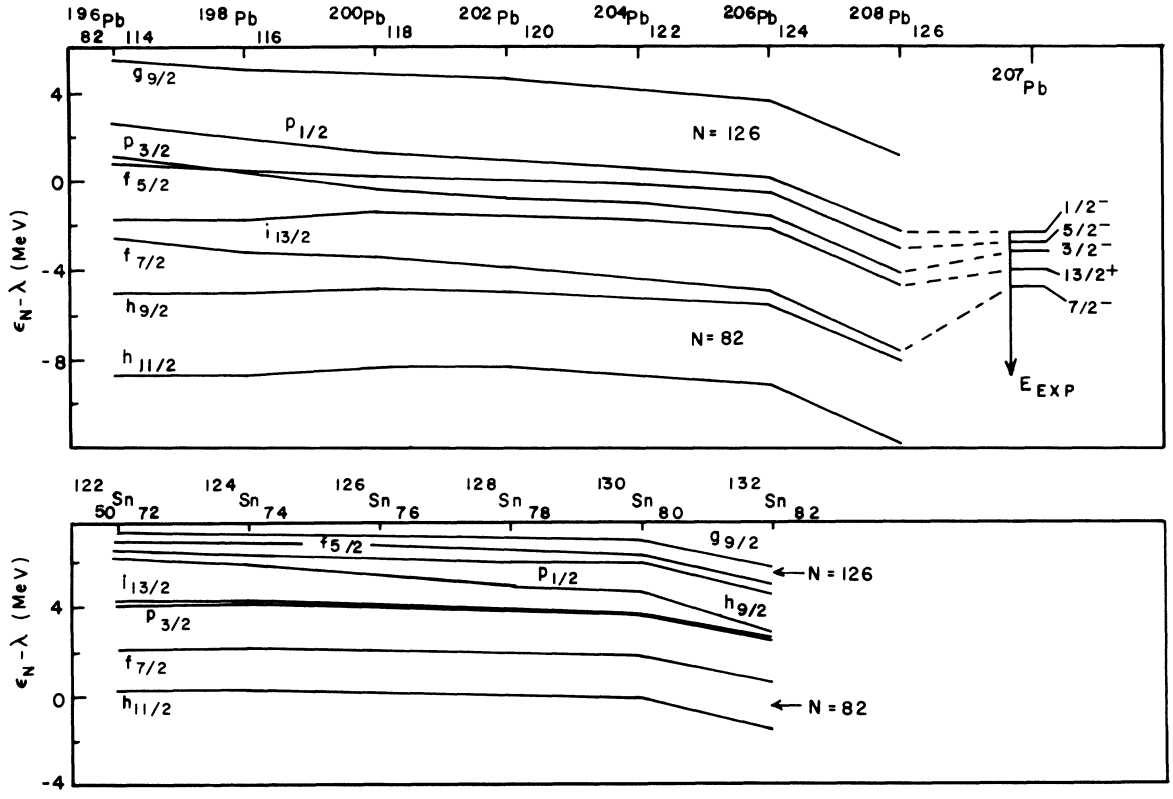

FIG. 16. HFB neutron Hartree-Fock single-particle energies $\epsilon_n - \lambda$ relative to the Fermi energy. The upper part of the figure is for N and Z values for Pb nuclei, while the lower part is for Sn. The experimental ^{207}Pb levels are also shown (inverted since this is a one neutron hole nucleus) for comparison.

We, of course, hope that this procedure will lead to results which would resemble those of a complete Hartree-Fock-Bogoliubov calculation. That is, we hope that the self-consistent changes (with N and Z, and with deformation and rotation) which would occur in an unrestricted HFB calculation would be due primarily to changes in the orbits and occupation probabilities of the valence particles.

To test this hypothesis we have solved the HFB equations with the same core energies as used in the rare-earth calculations for the spherical magic and semimagic $_{82}$Pb, $_{50}$Sn, $N=126$, and $N=82$ nuclei. Thus we can determine first if reasonable single-particle energies result for these spherical nuclei near the ends of our valence region, and furthermore determine if the changes of the pairing and Hartree fields with N and Z are well represented by the changes induced by the valence particles alone.

In Fig. 16 are shown the resulting neutron Hartree-Fock energies for the $_{82}$Pb and $_{50}$Sn isotopes relative to their respective Fermi energies together with the experimental ^{207}Pb spectrum. Notice that the two sets of levels are quite different showing large changes in the field from Pb to Sn. In particular for Pb, the energy gap and correct sequence of levels below $N=126$ is well reproduced. The Sn neutron levels show no energy gap at $N=126$, but do have a large enough gap at $N=82$ to make $^{132}_{50}\mathrm{Sn}_{82}$ a doubly magic nucleus with vanishing pairing. There is then reasonable accord with experiment for both Pb and Sn isotopes, and the large self-consistent shifts produced by the valence interactions are reasonable. (The experimental low lying levels of the odd Sn isotopes, not shown, include the $h_{11/2}$ level and also the $s_{1/2}$ and $d_{3/2}$ levels below $N=82$ and not included in the valence space.)

The neutron Hartree-Fock energies for $N=126$ and $N=82$ nuclei are shown in Fig. 17. For all the $N=126$ nuclei, 126 corresponds to a magic gap with $\Delta_n=0$, while for the $N=82$ nuclei, 82 has a gap with $\Delta_n=0$ for all the proton numbers shown. This is in agreement with a variety of data showing these to be magic numbers. Also the $N=83$ nuclei all are observed to have a $\frac{7}{2}^-$ ground state and in a number of cases a $\frac{9}{2}^-$ as a low excited state in agreement with the calculated level sequence.

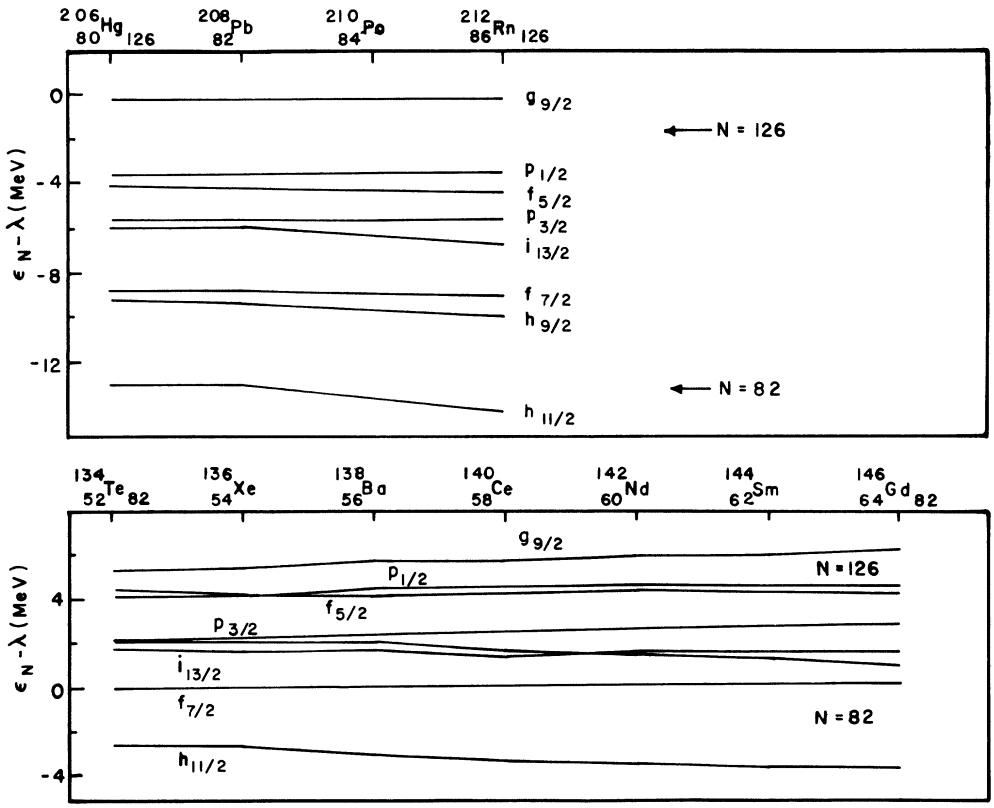

FIG. 17. HFB neutron Hartree-Fock single-particle energies for $N=126$ nuclei in the top figure and $N=82$ nuclei below.

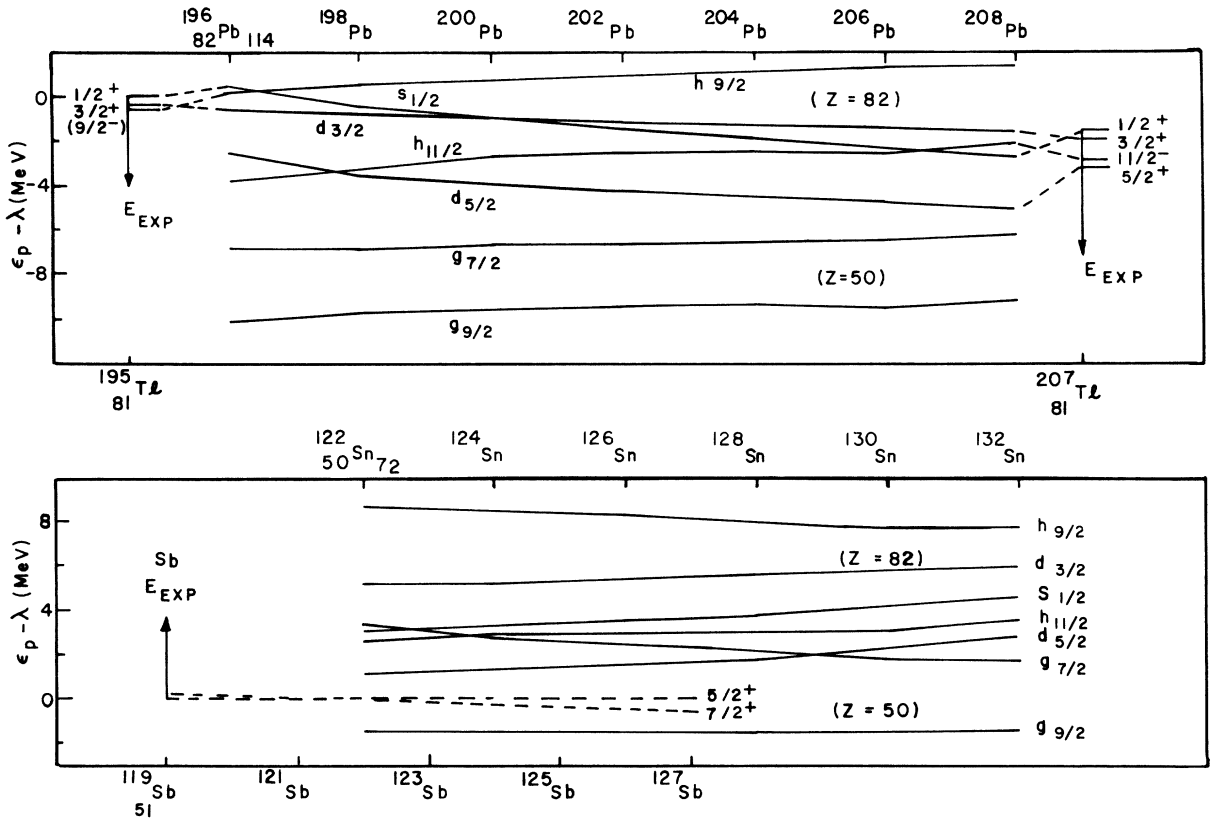

FIG. 18. HFB proton Hartree-Fock single-particle energies for Pb and Sn nuclei. Also shown are the experimental spectra for $^{195}_{81}$Tl and $^{207}_{81}$Tl (inverted) and for a sequence of odd mass $_{51}$Sb nuclei.

Therefore, the force within the valence shells reproduces quite well the details of the neutron level spacings from well below to well above the rare-earth region where it is being used.

The situation for the proton levels is similar. Figure 18 shows the proton Hartree-Fock energies for a sequence of even $_{82}$Pb and $_{50}$Sn isotopes together with some experimental $_{81}$Tl and $_{51}$Sb levels.

The proton gap at $Z=50$ is reproduced, the Δ_p values being less than 100–200 keV. The experimental $_{51}$Sb levels show that the trend of falling $g_{7/2}$ and rising $d_{5/2}$ with increasing N is reproduced, but the isotope for which these levels coincide (as in $^{121}_{51}\mathrm{Sb}_{70}$) is $N=78$ in the calculated spectra, while it is $N=70$ experimentally.

The proton gap at $Z=82$ for the Pb isotopes is seen to be rather N dependent. From $N \geq 118$, $Z=82$ is magic with $\Delta_p \approx 300$ keV for $N=118$ and going quickly to zero for the heavier Pb isotopes. But the $Z=82$ gap disappears completely by $N=114$, i.e., for $^{196}_{82}\mathrm{Pb}_{114}$ with the proton $h_{9/2}$ and $s_{1/2}$ levels nearly degenerate. This is in agreement with the observed magic character of the Pb isotopes with $N>118$ (for example on the basis of their high excitation energy for the first 2^+ state).

The disappearance of the proton gap for smaller neutron numbers is consistent with the observation in all the odd $_{81}$Tl isotopes with $N \leq 120$ of a low lying $\frac{9}{2}^-$ whose energy decreases with decreasing neutron number.

The relative spacing of the proton Hartree-Fock levels of the $N=126$ nuclei all look very much like those of $^{208}_{82}\mathrm{Pb}_{126}$ and the proton levels of the $N=82$ nuclei all look very much like those of $^{132}_{50}\mathrm{Sn}_{82}$, so they are not shown in a separate figure. In both cases the spacings between levels do not depend very much on the Z value. This is in agreement with the spins of the observed low energy states for the odd Z semimagic nuclei.

The Hartree-Fock-Bogoliubov calculations treat self-consistently both the Hartree-Fock field and the pairing field, and we stress the fact that the same force in the same space is used to calculate both these self-consistent fields.

For the magic spherical nuclei, the pairing correlations vanish as expected. For spherical semimagic (Sn, Pb, $N=82$, and $N=126$) nuclei we compare the HFB pairing with experiment in Figs. 19 and 20. In these figures, the experimental odd-even mass difference defined in (4.15) and (4.16)

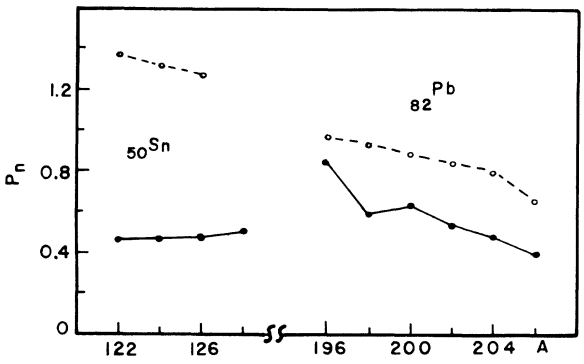

FIG. 19. Experimental odd (N) even mass difference (dashed line) vs smallest neutron quasiparticle energy E_i (minimum) (solid line) for Pb and Sn nuclei.

is plotted together with the lowest quasiparticle energy of the HFB calculation. For the Sn nuclei for which there is experimental mass data available, $N \leq 76$ and thus since the core has $N=70$, the space is too restricted for the buildup in HFB of a reasonable neutron pairing gap. This explains the low HFB quasiparticle energies for Sn. Likewise for $N=126$, the protons with $Z \geq 84$ are filling the last active orbit and the proton gap is small.

For the Pb and $N=82$ nuclei shown, the neutrons and protons, respectively, are well within the active space and reasonable pairing is observed. As with the rare-earth nuclei, the neutron Δ's are smaller than those of the protons by a greater amount than observed experimentally. While the proton HFB results agree well with experiment, the neutron HFB results are too low by about 30–40%.

In summary, it has been shown that except for the edges of the valence space, where only a very small number of particles (or holes) are free to move, both the Hartree-Fock field and the pairing field including their dependence on N and Z are in semiquantitative agreement with experiment for both spherical and deformed nuclei.

VI. CONCLUSIONS

As an effective interaction suitable for use in the rare-earth region, the bare G matrix elements derived from the Reid soft-core potential have been calculated. It was demonstrated that G has only a weak dependence on the starting energy ω, so that a single effective interaction using an average ω is suitable for the entire rare-earth region. For these heavy nuclei the effect of the Pauli operator Q is large so that G differs strongly from the reference G matrix G_{ref}. The use of an isospin independent Pauli operator and one-body oscillator length does not introduce a large error, but the combined effect probably produces a neutron-neutron effective interaction which is somewhat too weak.

This effective interaction is used in an HFB calculation in a large valence space (the fixed core has 40 protons and 70 neutrons furnishing fixed spherical single-particle energies) to calculate the ground state properties of a number of rare-earth nuclei. Deformations and pair gaps are both determined by the G matrix. The systematic variation with N and Z of the experimental single-particle energies, the β_2 and β_4 deformations, and the proton and neutron pairing gaps are generally reproduced. The magnitude of the β_2 deformations are somewhat too small presumably owing to the omission of the $Z=40$, $N=70$ core contribution. The proton pairing gap is of a reasonable magnitude, but the neutron pairing is a bit too small, probably due to the isospin independent single-particle oscillator parameter which leads to too large a neutron radius and thus to a weakened n-n interaction. The most serious discrepancy (for the subsequent calculation of high spin states) is that the calculated prolate-oblate energy differences are probably too small by several MeV.

As a further test of the range of validity of the force the same effective interaction and fixed core energies are used in an HFB calculation for the spherical semimagic nuclei with $N=82$ and 126 and $Z=50$ and 82. The resulting single-particle spherical levels move significantly over this large mass range and some level crossings occur. The resulting level energies and their mass dependences are consistent with the experimental trends.

Although suggested improvements (e.g., to increase the effective neutron interactions) are being considered, the presented results are in sufficient agreement with ground state properties

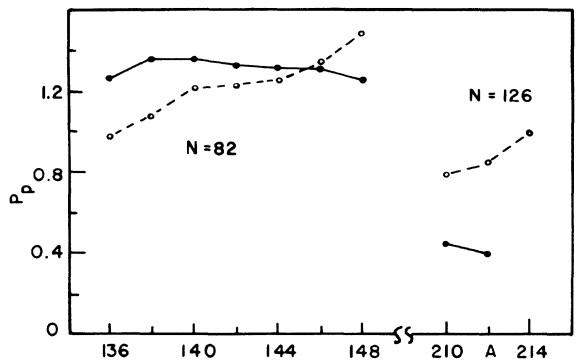

FIG. 20. Experimental odd (Z) even mass difference (dashed line) vs smallest proton quasiparticle energy E_i (minimum) (solid line) for $N=126$ and $N=82$ nuclei.

over a broad range of nuclei in the rare-earth region to provide a starting point for excited state, high spin calculations, with the exception of the very neutron deficient isotopes for which the oblate-prolate energy difference is still a problem. Some high spin calculations have already been made on this basis[35] and a more detailed presentation will be furnished later.[21]

---

*Work supported, in part, by the National Science Foundation.

†Work supported, in part, by the U.S. Energy Research and Development Administration.

‡Present address.

[1]R. V. Reid, Ann. Phys. (N.Y.) 50, 411 (1968).

[2]K. Kumar and M. Baranger, Nucl. Phys. A110, 529 (1968).

[3]M. Beiner, H. Flocard, N. V. Giai, and P. Quentin, Nucl. Phys. A238, 29 (1975).

[4]J. P. Vary and S. N. Yang, in *Proceedings of International Topical Conference on Effective Interactions and Operators in Nuclei*, edited by B. R. Barrett (University of Arizona Press, Tucson, 1975), Vol. 1, p. 22; J. P. Vary and S. N. Yang (unpublished).

[5]B. R. Barrett, R. G. L. Hewitt, and R. J. McCarthy, Phys. Rev. C 3, 1137 (1971).

[6]T. Hamada and I. D. Johnston, Nucl. Phys. 34, 382 (1962).

[7]B. R. Barrett, R. G. L. Hewitt, and R. J. McCarthy, Nucl. Phys. A184, 13 (1972).

[8]M. Baranger, *1962 Cargese Lectures in Theoretical Physics* (Benjamin, New York, 1963).

[9]B. Banerjee, H. J. Mang, and P. Ring, Nucl. Phys. A215, 366 (1973).

[10]C. Gustafson, I. L. Lamm, B. Nilsson, and S. G. Nilsson, Ark. Fys. 36, 613 (1966).

[11]D. Bes and R. Sorensen, *Advances in Nuclear Physics* (Plenum, New York, 1969), Vol. 2.

[12]P. D. Barnes, E. R. Flynn, G. J. Igo, and D. D. Armstrong, Phys. Rev. C 1, 228 (1970).

[13]J. H. E. Mattauch, W. Thiele, and A. H. Wapstra, Nucl. Phys. 67, 1 (1965).

[14]M. Conjeaud, S. Harar, and Y. Cassagnou, Nucl. Phys. A117, 449 (1968).

[15]Nucl. Data Sheets, nuclear level schemes $A=45$ through $A=257$.

[16]B. L. Cohen, R. H. Fulmer, A. L. McCarthy, and P. Mukherjee, Rev. Mod. Phys. 35, 332 (1963).

[17]A. L. Goodman, Ph.D. thesis, Berkeley, 1969 (unpublished) [UCRL Report No. UCRL-19514 (unpublished)].

[18]A. L. Goodman, Nucl. Phys. A186, 475 (1972).

[19]H. Flocard, P. Quentin, A. K. Kerman, and D. Vautherin, Nucl. Phys. A203, 433 (1973).

[20]U. Gotz, H. C. Pauli, and K. Alder, Nucl. Phys. A192, 1 (1972).

[21]A. L. Goodman (unpublished).

[22]G. E. Brown and T. T. S. Kuo, Nucl. Phys. A92, 481 (1967).

[23]K. E. G. Lobner, M. Vetter, and V. Honig, Nucl. Data A7, 495 (1970).

[24]W. H. Bassichis, B. A. Pohl, and A. K. Kerman, Nucl. Phys. A112, 360 (1968).

[25]A. H. Shaw and J. S. Greenberg, Phys. Rev. C 10, 263 (1974).

[26]H. J. Wollersheim, W. Wilcke, and T. W. Elze, Phys. Rev. C 11, 2008 (1975).

[27]I. Y. Lee, J. X. Saladin, J. Holden, J. O'Brien, C. Baktash, C. Bemis, P. H. Stelson, F. K. McGowan, W. T. Milner, J. L. C. Ford, R. L. Robinson, and W. Tuttle, Phys. Rev. C 12, 1483 (1975).

[28]S. G. Nilsson, C. F. Tsang, A. Sobiczewski, Z. Szymanski, S. Wycech, C. Gustafson, I. L. Lamm, P. Moller, and B. Nilsson, Nucl. Phys. A131, 1 (1969).

[29]H. Flocard, P. Quentin, and D. Vautherin, Phys. Lett. 46B, 304 (1973).

[30]A. Bohr and B. R. Mottelson, *Nuclear Structure* (Benjamin, New York, 1969), Vol. 1, p. 169.

[31]A. H. Wapstra and N. B. Gove, Nucl. Data A9, 267 (1971).

[32]V. A. Kravtsov and N. N. Skachkov, Nucl. Data A1, 491 (1966).

[33]K. Way and M. Wood, Phys. Rev. 94, 119 (1954).

[34]W. Ogle, S. Wahlborn, R. Piepenbring, and S. Fredriksson, Rev. Mod. Phys. 43, 424 (1971).

[35]A. L. Goodman and J. P. Vary, Phys. Rev. Lett. 35, 504 (1975).

[36]R. L. Becker, in *Proceedings of the International Topical Conference on Effective Interactions and Operators in Nuclei, Tucson, June 1975* (see Ref. 4); in *Lecture Notes in Physics*, edited by B. R. Barrett (Springer-Verlag, Heidelberg, 1975), Vol. 40.

[37]R. L. Becker, A. D. MacKellar, and B. Morris, Phys. Rev. 174, 1264 (1968).